Rheological Modelling of Asphalt Viscoelasticity

by

Evan Taylor Kohut

A thesis submitted in partial fulfillment of the requirements for the degree of

Master of Science

in

Chemical Engineering

Department of Chemical and Materials Engineering
University of Alberta

Abstract

The rheology of asphalt binders is an important factor in the design and construction of roads. As polymer modification is now often required to meet performance demands, the rheological behaviour of the binders has become increasingly complex. Within the past decade, a new method to evaluate these binders and their viscoelasticity has emerged – the Multiple Stress Creep Recovery (MSCR) test.

This thesis introduces a simple, lowest-order rheological model — the Standard Linear Fluid (SLF) model — that correctly predicts the MSCR response. It is shown that the SLF parameters can be obtained via a frequency sweep (involving *small deformations*) with a Dynamic Shear Rheometer. Furthermore, these parameters can be used to distinguish between polymer-modified and unmodified asphalts, just as a MSCR test can.

Although the SLF model has all the correct qualitative features, it significantly under-predicts the amount of strain that was recovered in an MSCR test. This discrepancy is attributed to the non-linearity of the material properties. Specifically, the SLF model parameters are determined from small-strain frequency sweeps, while the MSCR test involves large deformations — when non-linearities in material properties begin to appear.

An adjustment was made to the elastic element of the SLF model to account for non-linearity in the form of a hyperelastic Mooney-Rivlin solid. This improved the prediction for the recovery portion of the MSCR test considerably, but still not enough to agree with the experimental results at the cost of two additional parameters.

Acknowledgements

First, I must thank my supervisor, Dr. Tony Yeung, for all his support and guidance throughout this research. The patience he had with me after some of my mistakes and questions will not be forgotten. His calm and collected demeanour helped immensely during the moments where I was unsure of myself or our results. I would be content if I ended up becoming half the person he is (or his supervisor!).

In addition, I would also like to thank my supervisory committee members, Dr. Neda Nazemifard and Dr. Leila Hashemian for their time and feedback. Constructive criticism is always greatly appreciated, especially when it comes to my writing. I must also thank Artin Afacan for Chairing my examination, as well as the many conversations during my time as an undergrad student that sparked my interest in graduate studies.

Lastly, I would like to extend my thanks to those who contributed to this work externally. McAsphalt for providing the asphalt binders and Gecan for access to the experimental equipment needed.

Table of Contents

List of Tables

List of Figures

Chapter 1: Introduction

1.1 Asphalt Usage and Demand

Rheology is the study of how materials deform and flow under applied forces. In this thesis, the rheological properties of "asphalt binder," a material commonly used in road construction and preservation, will be examined. The process of paving roads requires mixing asphalt binder with various sizes of aggregates (i.e. small pieces of rocks) to form "asphalt concrete." The binder in this mixture acts as a glue and typically accounts for (roughly) 5% of the total weight by mass. As the binder is extremely viscous, it must be sufficiently heated to allow for a coating over the aggregates. After the mixture is formed and laid down as paved road, it is allowed to cool and 'set,' so that the road can gain the elasticity needed to resist breaking down under traffic loads. Both the viscosity and elasticity of the binder are crucial rheological parameters that need to be considered and adjusted when designing any roadway. In Canada alone, there are over 1.1 million kilometers of two-lane equivalent roads, of which approximately 40% is paved [1]. Additionally, there are nearly 7 million kilometers or roadway in the US, of which approximately 95% is paved [2], [3]. Clearly a substantial volume of asphalt binder is required to build and maintain the vast road networks across North America. With this idea in mind, it is important to realize that not all asphalt binders should have the same rheological properties; they must be tailored for their specific application (e.g. different ranges of temperature or traffic loads).

Currently, the most common method of evaluating and distinguishing asphalt binders from each other is known as the Performance Grading (PG) system. A PG characterization is specified by two temperatures: hot and cold. Thus, a material identified as PG 58-28 has been determined to be suitable for road (<u>not air</u>) temperatures between +58°C and −28°C. Naturally, different locations experience different climates. Therefore, the location of a roadway is often the determining factor for the type of binder that is necessary for the job. It is reasonable to expect that a road constructed in the desert climate of Arizona requires different asphalt properties than one constructed in the frigid regions in Northern Canada. To pave roads across such extremes of climates, it is clear that the rheology of the asphalt (the glue which binds together the rocks) must be well understood. However, on closer

1

examination of how material testing has progressed over the past decades, one realizes that the PG (Performance Grading) system, although clearly an attempt at scientific rigor, has been quite superficial in its characterization of asphalt binder rheology.

1.2 Origins of Asphalt Grading

The first known method of experimental asphalt grading was adopted in the early 1900's by the American Society for Testing Materials (ASTM), Committee D04, for road and paving materials [4]. In this time period, the usage of bituminous and tar products for roads was steadily increasing. As motorized vehicles were becoming more popular across America, the demand for roads that could support vehicles that were much faster and heavier than horse carriages increased dramatically. At the time, the bituminous and tar materials used as binders in road construction had also other applications, such as roofing and waterproofing [4]. The development of the "Penetration test" was done in part to determine what application a given asphalt was suitable for. This test, quite simply, measures how deep a needle of a certain weight (100g) penetrates a sample over a fixed duration of time (5s) at 25°C [5]. The penetration depth is loosely correlated with the viscosity of the binder: less depth is equated to higher viscosity. However, this correlation is only empirical, and the test is not performed at temperatures that road surfaces typically experience.

The D04 Committee, having recognized the shortcomings of the penetration test, developed Viscosity Grading in the 1960's, although the methods were not adopted by ASTM until 1975 [4]. Viscosity testing measures and converts the time it takes a sample to fill a calibrated capillary into a viscosity (assuming, inherently, that the material is Newtonian). Two test methods were developed: viscosity of asphalts by vacuum capillary viscometer and kinematic viscosity (gravity induced) measurement [6], [7]. These tests take place at 60°C and 135°C respectively. The measuring of a viscosity parameter at approximate road surface and mixing temperatures allow for better characterization of asphalt binders. Additionally, when combined with Penetration Grading, some information is gained over a large range of temperatures. However, no information on the performance of the binders in cold temperatures can be obtained using either method.

There are some similarities between the Penetration and Viscosity protocols, namely the evaluation of the binder before and after ageing. Ageing is a term used to describe the oxidation process that the asphalt undergoes over time. The terminology often used together with ageing is "hardening." Although this may provide an intuitive description of how the material has changed, no quantification of the performance of a binder can be provided by such terminology. To say one binder sample is "harder" than another does not always indicate how they will perform relative to each other. In addition, samples with similar penetration and viscosity values could perform quite differently in the field. Obviously, it is difficult to predict the performance of materials via needle or capillary tests that do not capture what occurs in the field. Although viscosity is a fundamental engineering parameter, clearly there was a gap in the ability to characterize the rheology of these materials, especially at the conditions they were expected to perform in. This gap would eventually be addressed using rheometers as advancements in instrumentation were made.

1.3 Performance Grading

1.3.1 Development of Performance Grading

As mentioned earlier, the Performance Grading (PG) system provides hot and cold temperature limits for an asphalt binder. This system was developed during the 1980's and 1990's by the Strategic Highway Research Program (SHRP), specifically for performance-based asphalt binder tests. It was adopted as standard protocol for evaluating asphalt binders in 1998, replacing the penetration and viscosity grading systems [4].

In the PG system, a dynamic shear rheometer (DSR) is used to evaluate the viscous and elastic properties of the binder at the high temperature limit [8]. At low-end temperatures, a bending beam rheometer (BBR) is used to measure the stiffness and ability to relax stress in the binder [9]. These rheometers introduced a significant improvement in the way materials were characterized, as they provided direct rheological information (stresses as functions of strains and rates of strain) instead of correlations (depth of a needle, time to flow in capillary). Additionally, binders could now be tested in the entire temperature range of practical interest. This temperature range is expressed in the grading designation (e.g. the PG 58-28 that was discussed earlier).

Grading designations in the PG system are separated by a 6°C intervals for both the high and low temperature limits. The high-end temperatures begin at 46°C and increase up to 82°C, while the low-end temperatures range from −10°C to −46°C. Figure 1.1 shows the possible combinations of PG grades recognized in the AASHTO M320 PG Specification Table [10]. It is worth noting that not all grade combinations in the range listed are possible. For example, there is no listing for a PG 76-46. Typically, a hotter high-end temperature is paired with a warmer low-end temperature (e.g. PG 76-16). This is because the properties that let binders perform better in hotter weather ("stiff," more difficult to deform) are also undesirable for colder weather (too "stiff" and can lead to cracking in cold weather). These opposing conditions force road designers to consider both ends of the weather extreme when balancing out expected asphalt binder performance. A short briefing of the protocols used in PG testing will outline how designers of the PG standard attempt to accomplish this and where they ultimately fall short in characterizing asphalt binder rheology.

Performance Grades

Max. Design Temp.	PG 46	PG 52	PG 58	PG 64	PG 70	PG 76	PG 82
Min. Design Temp.	-34 -40 -46	-10 -16 -22 -28 -34 -40 -46	-16 -22 -28 -34 -40	-10 -16 -22 -28 -34 -40	-10 -16 -22 -28 -34	-10 -16 -22 -28 -34	-10 -16 -22 -28 -34

Original

≥230 °C	**Flash Point**
≤ 3 Pa-s @ 135 °C	**Rotational Viscosity**

DSR G*/sin δ (Dynamic Shear Rheometer)

≥ 1.00 kPa	46	52	58	64	70	76	82

(Rolling Thin Film Oven) RTFO, Mass Change ≤ 1.00%

DSR G*/sin δ (Dynamic Shear Rheometer)

≥ 2.20 kPa	46	52	58	64	70	76	82

(Pressure Aging Vessel) PAV

20 hours, 2.10 MPa	90	90	100	100	100(110)	100(110)	100(110)

DSR G*sin δ (Dynamic Shear Rheometer) Intermediate Temp. = [(Max. + Min.)/2] + 4

≤ 5000 kPa	10 7 4	25 22 19 16 13 10 7	25 22 19 16 13	31 28 25 22 19 16	34 31 28 25 22 19	37 34 31 28 25	40 37 34 31 28

BBR S (creep stiffness) & m-value (Bending Beam Rheometer)

S ≤ 300 MPa m ≥ 0.300	-24 -30 -36	0 -6 -12 -18 -24 -30 -36	-6 -12 -18 -24 -30	0 -6 -12 -18 -24 -30	0 -6 -12 -18 -24	0 -6 -12 -18 -24	0 -6 -12 -18 -24

If BBR m-value ≥ 0.300 and creep stiffness is between 300 and 600, the Direct Tension failure strain requirement can be used in lieu of the creep stiffness requirement.

DTT (Direct Tension Tester)

ε_f ≥ 1.00%	-24 -30 -36	0 -6 -12 -18 -24 -30 -36	-6 -12 -18 -24 -30	0 -6 -12 -18 -24 -30	0 -6 -12 -18 -24	0 -6 -12 -18 -24	0 -6 -12 -18 -24

Figure 1.1 PG Specification Table M320. Used for outlining requirements needed to grade an asphalt. The first two rows outline the possible grades that can be given to an asphalt binder. The remainder of the table shows a temperature requirement corresponding to a specific test (rows) for a specific PG grade (columns).

1.3.2 Temperature Limit Determinations

The PG system is a protocol for determining the appropriate temperature at which an asphalt should function. It is based on two notions:

- An asphalt should be sufficiently "stiff" to function as a binder.

- Generally, an asphalt becomes less "stiff" as the temperature is increased.

The aim of the PG system is therefore to identify the temperatures at which the asphalt meets its "minimum stiffness requirement" for the high temperature limit and "maximum stiffness requirement" for the low temperature limit. A sketch of the principle behind the PG system is shown for the high limit in Figure 1.2 below:
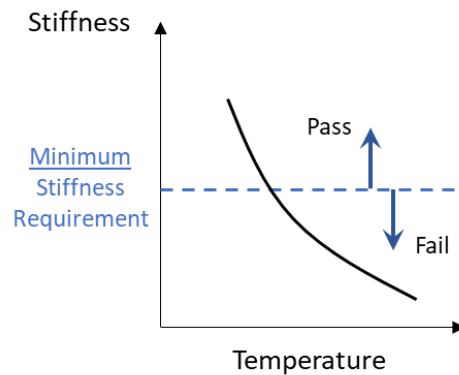
Figure 1.2 A sketch outlining the basis of the PG system high temperature determination.

To determine the high temperature limit, a DSR (dynamic shear rheometer) is used with an angular frequency of 10 rad/s at varying temperatures [8]. Like the Penetration/Viscosity system, this protocol is performed before and after ageing. The limiting temperature is selected from the PG temperature that meets the minimum stiffness requirement at both ageing conditions.

This limiting temperature is intended to serve as an estimate to how well the material will resist against "rutting". Rutting is the term used to describe the permanent deformation from traffic loads into a pavement structure, as shown in Figure 1.3. In order to resist rutting, a binder should be stiff enough that it does not deform a significant amount under traffic loads and have some elasticity to recover the small amount of deformation that cannot be

prevented. However, as we will discuss shortly, there is reason to believe that this high temperature limit is a bad predictor of rutting and that another testing method exists that predicts rutting more accurately.

Figure 1.3 An example of extreme rutting in a pavement structure [11].

To determine the low temperature limit, a BBR (bending beam rheometer) is utilized on material that has undergone further ageing [9]. The additional oxidizing is done in part so that BBR testing is performed under conditions that mimics the long-term oxidation of roads that become susceptible to cracking. Measurements from the BBR identify the stiffness and the material's ability to relax stress through a creep test under a 100g load. The limiting temperature is selected as the PG temperature that meets the maximum stiffness (and a minimum deflection rate) requirement after 60s of loading. This limiting temperature estimates when a binder will exhibit thermal cracking.

The PG system appears to be more scientific than the traditional penetration-viscosity tests. However, on closer inspection, this protocol turns out to be a misrepresentation of the principles of rheology.

1.4 Shortcomings of PG Designations

Current asphalt binder testing protocol uses the DSR and BBR to gather a small amount of rheological information in the temperature range that the material is expected to perform in. While this may seem adequate enough to ensure materials are being evaluated for varying weather, there are problems with using temperature as the basis for performance that need to be addressed.

To summarize both the high and low temperature limit procedures: only one angular frequency/loading input is used per rheometer, while temperature is varied until a specific failing criterion is met. In a way, the PG system is just an extension of the Pen/Visc system. Of course, using a machine to control the shearing and deforming of a sample while measuring the response in real time is a significant improvement over correlating the depth that a needle penetrates. However, by limiting these machines to just one rate or load, we are not fully utilizing the machine to understand the material the best we can. In this sense, the PG system is essentially trusting these single inputs to accurately predict performance, just as the Pen/Visc system previously did.

Furthermore, the analysis performed by SHRP in developing the PG system was largely based on "neat" (unmodified) asphalts [12]. During the transition from the Pen/Visc testing to PG, asphalt binders were becoming increasingly "modified." In this context, the 'modification' of an asphalt binder is the addition of chemicals that affect its performance. Figure 1.4 shows a table of modified and unmodified PG designations. Both value-adding and subtracting additives exist in the asphalt industry. For example, a product may meet specification for a PG 58-28 with a true grade (predicted fail temperatures) of PG 62-32. At the high-end, there is 4°C of extra performance that is not reflected in the reported PG grade. To save costs, a supplier may add some form of diluent that reduces the true grade to a PG 59-30. In this case, the binder still meets the specification for a PG 58-28, but the integrity and rheological performance of the binder has been compromised. Specifically, the addition of diluent will likely hinder the pavement performance as it offers no elasticity to the binder. This results in a product the performs worse than its PG designation.

High Temperature, °C

Low Temperature, °C	52	58	64	70	76
-16	52-16	58-16	64-16	70-16	76-16
-22	52-22	58-22	64-22	70-22	76-22
-28	52-28	58-28	64-28	70-28	76-28
-34	52-34	58-34	64-34	70-34	76-34
-40	52-40	58-40	64-40	70-40	76-40

= Crude Oil

= High Quality Crude Oil

= Modifier Required

Figure 1.4 A table classifying PG designations based on whether they are modified [13].

On the other hand, there are instances where the product needs to be enhanced. The most common way of achieving this is by using polymers designed to improve low-end performance. Polymer modified asphalts (PMA) are widely used across North America because they can improve the low temperature grade without sacrificing a grade on the high end. In general, additives that help one side of the temperature grade will compromise the other. However, a field comparison between PMA and neat PG 64-22 showed the PMA resisted rutting and showed less susceptibility to thermal cracking than the unmodified version of the same grade [14], [15]. Other studies demonstrated that PMA has less temperature susceptibility than neat asphalts at both high and low temperatures [16], [17]. It is clear from these studies that PMA performance can be superior to neat asphalts despite no indication from their PG grades.

This exposes a problem in evaluating asphalt binders using the PG system as it was not designed for modified asphalts. In particular, the grade designations do not reliably predict better performance. High-end temperature limits do not accurately predict which material will resist rutting to a greater degree. Likewise, low-end limits do not showcase the enhanced ability of PMA to resist thermal cracking compared to neat asphalts. The methodology of the PG system to evaluate a material based on performance at temperature ranges allows for

discrepancies to exist within the intervals. When deciding on performance, if the choice between PMA and neat asphalts is undeniably in favor of PMA, then it makes sense to establish criteria that determine the effect of the polymer on the asphalt rheology.

1.5 Beyond PG

1.5.1 PG Plus

The first attempt at establishing a criterion for PMA was "PG Plus" tests, developed in the late 1990's. Included in PG Plus protocol are three empirical tests: Toughness and Tenacity (T&T), Ductility, and Elastic Recovery. The procedure for all three tests involves a binder sample being stretched out at a fixed rate, usually at 25°C. In T&T and Ductility, the sample is stretched vertically or horizontally, respectively, until it splits into two pieces. For Elastic Recovery, the binder is only stretched a small distance and then cut in half. The amount of recoil over 1 hour is then measured as a percentage. For all three procedures, unmodified binders show almost no recovery or stretching ability while PMAs are able to stretch and recover a significant amount.

When comparing two PMA binders, there is no clear indication how performance is affected based on recovery amount or elongation length. The discrepancy in results between unmodified and polymer modified was obvious, but it was difficult to evaluate performance between two PMAs. Thus, these tests could only be used to establish the presence of polymer in an asphalt and are now generally viewed as obsolete due to recent advancements with DSRs and their utilization.

1.5.2 MSCR: Multiple Stress Creep Recovery

In recent years, many states and provinces have adopted the "multiple stress creep recovery" (MSCR) test as either an additional requirement or alternative to PG testing. It was first implemented in 2010 with the purpose of properly evaluating rutting susceptibility for polymer modified and unmodified asphalts [18]. The procedure for MSCR testing requires the DSR to perform cyclic loading on aged binder at a fixed temperature. A 0.1 kPa constant load is applied for 1 second; the asphalt is then allowed to recover under no stress for 9

seconds. This cycle is repeated for a total of ten loads, and then another ten cycles are performed at 3.2 kPa [19].

By using a high and a low level of stress, the effects of the polymer are being investigated across a range of possible excitations. Throughout the duration of the test, the shear strain amount is recorded as a function of time. This allows for a comparison of polymer activity between binders. Figure 1.5 shows an example of data for one cycle. Recall that "rutting" is used to describe permanent deformation. When evaluating multiple (modified or unmodified) binders, the results of the MSCR test can be used to directly show which will resist rutting more effectively. Specifically, the amount of non-recoverable shear strain (permanent deformation) and the percentage of strain that is recovered can be compared. Multiple studies have shown the improvement these two parameters provide in predicting rutting susceptibility compared to the PG and PG Plus requirements [20]. Intuitively, it makes sense to limit the maximum amount of permanent strain instead of requiring a minimum stiffness value. Likewise, it is more representative to impose a minimum recovery amount performed at expected road temperatures.
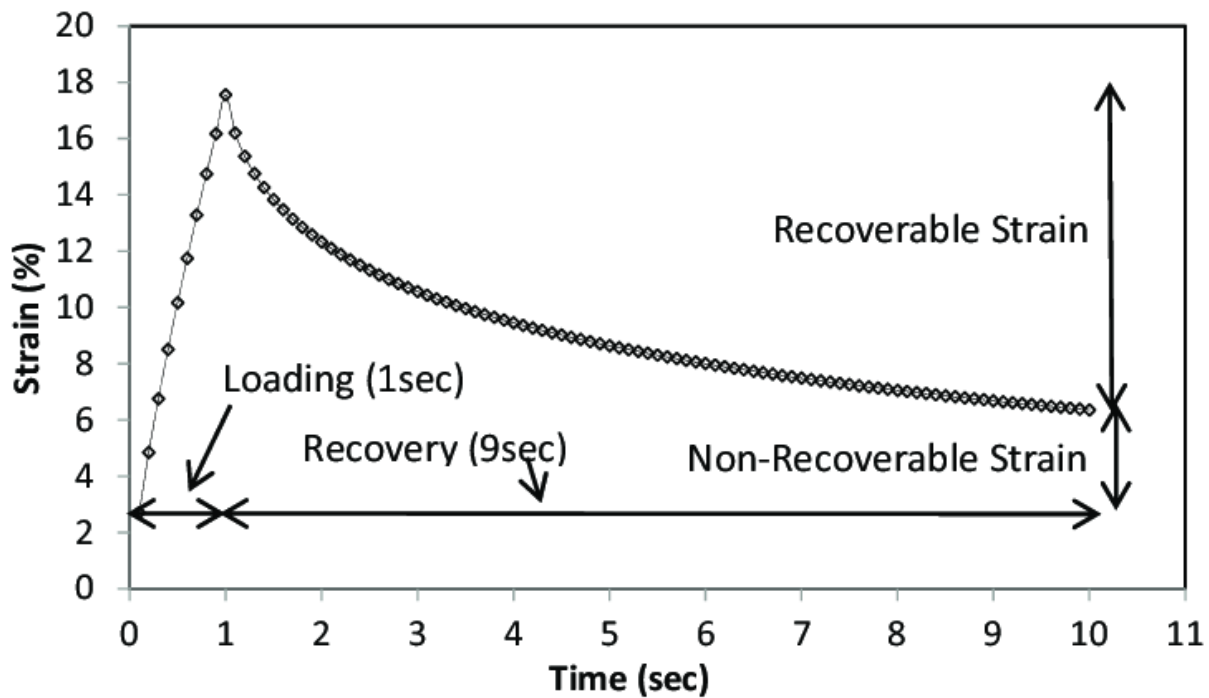
Figure 1.5 A plot showing the response of one cycle in the MSCR test [21].

10

There are two important features in this plot that form the basis of this thesis. First, the binder does not deform instantaneously at the onset of the load (at $t = 0$). Having a finite rate of strain indicates the binder has the characteristics of a liquid. Second, upon removal of the load (after 1 second), the binder recovers partially. The ability to recover indicates the characteristics of a solid material are also present. The presence of both solid and liquid like characteristics reveals that this binder is a *viscoelastic* material. It will be shown that viscoelasticity is not exclusive to polymer modified asphalts, but rather, viscoelasticity is inherent in all asphalt binders. To identify and quantify these characteristics properly, we must investigate asphalt binder rheology.

1.6 Rheology of Asphalt: A New Model

All discussion thus far has had to do with *grading*, which is based on very specific experiments (e.g. ASTM protocols). From the empirical results of these standardized tests, asphalt samples can be classified into different "grades," or more accurately, "temperature ranges." Throughout our review, the failure of the PG system (remember, still currently the most used) was outlined to be due to improperly characterizing rutting and thermal cracking ability amongst binders, whether they were modified or unmodified. However, the root cause of this failure lies within the inability to adequately characterize the rheology of the asphalt binder with only one external excitation. Although the MSCR protocol is an improvement in this regard (using multiple stresses) there is still much worthwhile information to gain about these materials.

If the external disturbance imposed on an asphalt binder is limited *only* to the penetration of a 100g needle, or shearing between two circular plates at a frequency of 10 rad/s, or ten cycles of 1-second long creep loads of 3.2 kPa, then the grading test results are all that is needed. Of course, in reality, the number of mechanical excitations that an asphalt can be subjected to is limitless. How, for example, would an asphalt respond to oscillatory stress by a DSR at 20 rad/s or if the MSCR protocol is changed to 5 seconds of stress followed by 5 seconds of recovery?

To truly understand the physical properties of asphalt, one needs to understand its *rheology*, which is the study of how a material deforms and flows under external excitations. It is common to use rheological models to predict the material response to these excitations. The aim of this thesis is to introduce a simple, lowest-order rheological model for asphalt binders — a model that is capable of properly characterizing their viscoelasticity and MSCR response.

1.7 About This Thesis

The focus of this thesis is to demonstrate the ability of the Standard Linear Fluid (SLF) rheological model to evaluate asphalt binders. Chapter 2 details the basic principles of rheology and examines the shortcomings of other rheological models, including one specifically for asphalt binders. Chapter 3 outlines the materials, experimental procedures and applications of the DSR. In Chapter 4, experimental results from fitting data to the SLF model are presented and discussed. Lastly, Chapter 5 will provide a summary of the findings from this research, as well as recommendations for future work and other applications of the SLF model.

Chapter 2: Principles of Viscoelasticity

2.1 Rheology and Linear Viscoelasticity

Rheology is the study of how materials *deform* and *flow* under external forces. It is common to associate deformation with solids, and flow with fluids. This, however, does not imply rheology is simply an umbrella term for the two traditional branches of science known as solid mechanics and fluid mechanics; rheology deals also with materials which have properties that are "hybrid" between solids and fluids (in addition to those with other complex behaviours — to be briefly mentioned in §2.1.4).

2.1.1 Viscoelastic materials

We begin our discussion with the two "extreme" cases in rheological behaviour, namely, the *perfect elastic solid* and *perfect viscous fluid*. Table 2.1 summarizes — and contrasts — the qualitative features of these two types of materials.

Table 2.1 Contrasts between *perfect elastic solid* and *perfect viscous fluid*.

Feature	Perfect Elastic Solid	Perfect Viscous Fluid
Memory of the original (i.e. undeformed) configuration:	Complete	None
Instantaneous deformation?	Allowed	Forbidden
Stresses are developed in the body to resist ...	strain (relative to original configuration), regardless of the *rate* of strain.	*rate* of strain, regardless of the amount of strain.
Additional details on the stresses of resistance:	They increase monotonically with strain, and vanish when the body is undeformed.	They increase monotonically with the rate of strain, and vanish when the body is at rest.

Despite the highly idealized features, these two models are very good approximations to the behaviours of many solids, liquids, and gases (particularly for substances of low molecular weights or with homogeneous microstructures). There are, however, equally numerous materials that do not conform to either of the two models in Table 2.1. As examples, a material may

(a) have complete memory of its original configuration, but cannot undergo instantaneous deformations; or

(b) have no memory if its original configuration, but can deform abruptly in response to sudden changes in the applied force.

Such materials, with features that are hybrid between perfect viscous fluids and perfect elastic solids, are collectively called *viscoelastic* materials. As a matter of semantics, in this thesis, we will designate a material as either "solid" or "fluid" based only on the first feature in Table 2.1, namely, its memory of the original configuration. Thus, the material in Example (a) is considered a viscoelastic solid, while that in Example (b) a viscoelastic fluid.

2.1.2 One-dimensional analogues in viscoelasticity

The stresses and strains mentioned in Table 2.1 are of course tensorial quantities; they are denoted σ_{ij} and ε_{ij}, respectively. To simplify the analysis, it is common in rheological studies to focus on only *one* — the most relevant — component of σ_{ij}, and on the corresponding component of ε_{ij}. With regard to what is "most relevant," the two common modes of excitation in material testing are *tensile loading* and *torsional shear*, as shown in Figure 2.1:

(a) Tensile test   (b) Torsional shear test
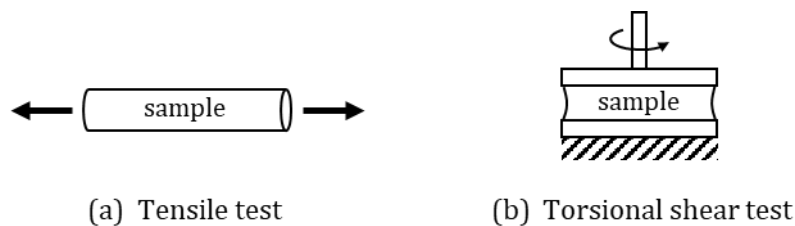
Figure 2.1 The two common modes of material testing: (a) Longitudinal loading along the axis of a cylindrical sample, and (b) torsional shearing of a sample that is placed between two parallel circular discs.

In terms of cylindrical coordinates (r, θ, z) — with the z-axis coinciding with the symmetry axes in Figure 2.1 — the most relevant stress and strain components are: $(\sigma_{zz}, \varepsilon_{zz})$ for tensile loading, and $(\sigma_{\theta z}, \varepsilon_{\theta z})$ for torsional shear. In the literature, the subscripts "zz" or "θz" are often omitted, leaving the stress and strain components appearing simply as σ and ε. (Unless additional information is provided, one would not know from this notation whether σ and ε result from tensile or torsional excitation.)

With the stress and strain tensors now reduced to single scalars (i.e. σ and ε), the next step is to propose *constitutive relations* in the form of

$$\sigma = \sigma(\varepsilon, \dot{\varepsilon}) \tag{2.1}$$

for different viscoelastic behaviours ($\dot{\varepsilon} = \mathrm{d}\varepsilon/\mathrm{d}t$ is the rate of strain). Viscoelasticity, as the name implies, is comprised of two fundamental and disparate material properties: viscosity and elasticity. To provide an "intuitive feel" for these two properties, they are often depicted in textbooks as springs (for elasticity) and dashpots (for viscosity), as shown in Figure 2.2:

Spring representing elasticity

Dashpot representing viscosity
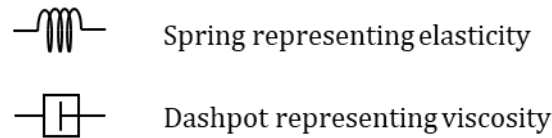
Figure 2.2 One-dimensional analogues of elasticity and viscosity.

The elements in Figure 2.2 invoke images of force-displacement relations in the longitudinal direction. However, it must be remembered that these elements are merely *one-dimensional analogues* and should not be interpreted in a strict, literal sense. The longitudinal force along the imaginary spring/dashpot is intended as a metaphor for the stress σ (with units of Pa), while the resulting longitudinal displacement is a metaphor for the strain ε (which is dimensionless). This analogy applies equally to the torsional shear situation (Fig. 2.1b), even though the actual process does not involve extension/compression in the longitudinal direction.

2.1.3 Linear viscoelasticity

Next, we discuss constitutive relations for viscoelastic materials. We begin with perfect elastic solids and viscous fluids. Referring to the last feature in Table 2.1, the statements suggest that

- For an elastic solid, a plot of σ vs ε would pass through the origin. The stress σ increases monotonically with ε, and the relation can in general be non-linear.
- For a viscous fluid, a plot of σ vs $\dot{\varepsilon}$ would pass through the origin. The stress σ increases monotonically with $\dot{\varepsilon}$, and the relation can in general be non-linear.

It is natural, as first approximation, to postulate linear relations. This leads to the well-known Hookean solid and Newtonian fluid:

$$\sigma = \begin{cases} G\,\varepsilon & \text{Hookean solid} \\[2ex] \mu\,\dot{\varepsilon} & \text{Newtonian fluid} \end{cases} \tag{2.2}$$

The parameters G and μ are, respectively, the shear elastic modulus and the shear viscous modulus (or simply "viscosity"); they are assumed to be independent of ε and $\dot{\varepsilon}$. In the literature, the symbol G is normally associated with *shear* deformation. The Hookean relation in eqn 2.2 is written in terms of G because, in this work, we rely on data generated by a torsional rheometer in which the sample is subject to simple shearing (as depicted in Figure 2.1b). [If material testing were done in a tensile mode, the appropriate elastic constant would be the Young's modulus — often denoted E.]

Hookean solid and Newtonian fluid (eqn 2.2) are the most basic forms of linear viscoelasticity. (Here, the word "linear" refers to the fact that ε and/or $\dot{\varepsilon}$ appear as first powers in the constitutive relations.) Other linear viscoelastic behaviours can be represented by combinations of these two basic elements. Returning to the two examples at the end of §2.1.1, the material in Example (a) can be modelled by placing an elastic spring in parallel with a dashpot, resulting in a *Kelvin-Voigt solid*, while the material in Example (b) is modelled by putting the spring and the dashpot in series, leading to a *Maxwell fluid*. A sketch of these two linear viscoelastic models is shown in Figure 2.3:
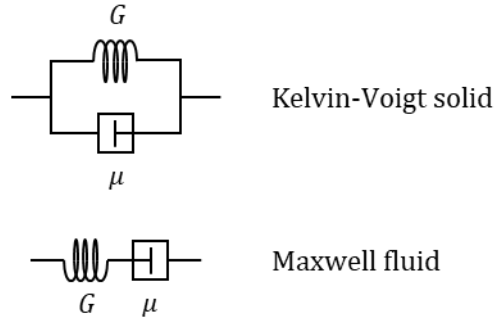
Figure 2.3 Two ways of combining a linear spring and a linear dashpot, resulting in the Kelvin-Voigt solid and the Maxwell fluid. Constitutive relations for the spring and dashpot are given in eqn 2.2.

Other models can be concocted by adding more springs and dashpots. For example, a "standard linear solid" is formed by placing an elastic spring in parallel with a Maxwell fluid, while a "standard linear fluid" results when a dashpot is connected in parallel with a Maxwell fluid (see Figure 2.4). The "Burgers model," with two springs and two dashpots, is formed by connecting a Kelvin-Voigt solid in series with a Maxwell fluid (sketch not included here).
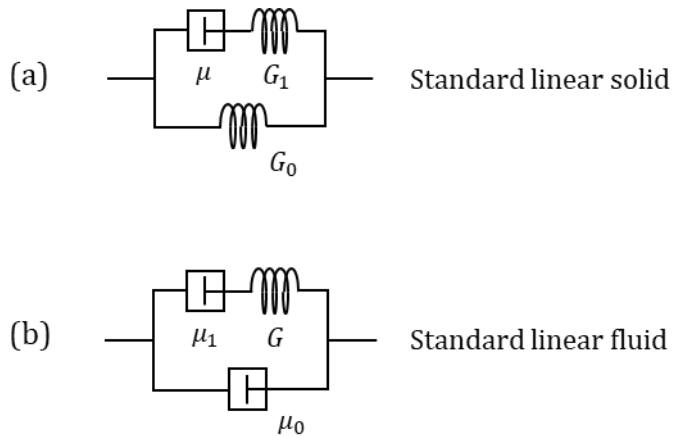
Figure 2.4 The so-called "standard linear solid" and "standard linear fluid" models.

It is clear that, as one continues to include more springs and dashpots in various combinations, it is possible to replicate any type of empirical stress-strain relation. However, we argue here that the purpose of modelling is not to fit empirical results to arbitrary accuracy by introducing an ever-increasing number of adjustable coefficients; rather, it is to capture the underlying physics with the *least* number of parameters.

17

In summary, one may think of linear viscoelasticity as "a language with only two alphabets": the linear spring (i.e. Hookean solid) and the linear dashpot (i.e. Newtonian fluid). Various linear viscoelastic models can be created by using different numbers of these elements and arranging them in different configurations.

2.1.4 Other branches of rheology

Linear viscoelasticity, discussed in the previous section, is not synonymous with rheology; it is a subset of the latter (arguably the most important one). Figure 2.5 shows how the general field of rheology is divided into its different branches. The following are brief descriptions of each category:

- Viscoelasticity involves combining perfect elastic solids and perfect viscous fluids (described in Table 2.1) in different arrangements to form rheological models. If the elastic and viscous relations are linear (as in eqn 2.2), we have *linear viscoelasticity*. If the constitutive relations were non-linear (e.g. as rubber undergoes large deformations), the theory would be called non-linear viscoelasticity.

- The theory of viscoplasticity was proposed to describe materials with a *yield stress* σ_y. Such materials behave as solids when the applied stress is below σ_y, and flow like fluids when the stress level exceeds σ_y. Many personal care products and food colloids are viscoplastic; two familiar examples are toothpaste and mayonnaise.

- Thixotropy refers to the phenomenon of time-evolving viscosity as the fluid structure undergoes spontaneous rearrangement on the colloidal or molecular scale. It should be noted that this time evolution in viscosity is *not* a result of external influences such as temperature or the applied stress. Dense suspensions of colloidal particles often exhibit thixotropic behaviours.

Rheology

Viscoelasticity   Viscoplasticity   Thixotropy
(i.e. time-dependent viscosity)

Linear
Viscoelasticity

Non-linear
Viscoelasticity

May include

- non-linear elasticity
  (e.g. hyperelastic materials)

- non-linear viscosity
  (e.g. shear thinning/thickening)

- Includes *linear elasticity* and *Newtonian fluid mechanics*
  as sub-branches
- Constitutive relations involve
  ➢ constant elastic and/or viscous moduli
  ➢ only *first powers* of ε_{ij}, σ_{ij}, and their
    time derivatives

Figure 2.5 Rheology and its different branches of study.

2.1.5 Linear viscoelastic model for asphalt

In this thesis, the theory of linear viscoelasticity will be used to model the rheology of asphalts. As discussed in §2.1.3, by combining springs and dashpots in various ways, one can come up with any number of complex models. However, in the interest of capturing the correct physics with the least number of parameters, we will consider only the models shown in Figures 2–4. Empirical results from the so-called MSCR test will be used as a guide to choosing the correct model. (Recall MSCR stands for "multiple stress creep recovery"; see §1.5.2.) Arguments in this subsection will be made in qualitative terms only.

Recall that the MSCR test involves (i) subjecting the material to a step change in stress at time $t = 0$, and (ii) dropping the applied stress abruptly to zero at time $t = t_0$. The resulting strain $\varepsilon(t)$ has two important features:

- The material does *not* deform instantaneously at $t = 0$, and

- beyond $t = t_0$, the material recovers partially — but not completely.
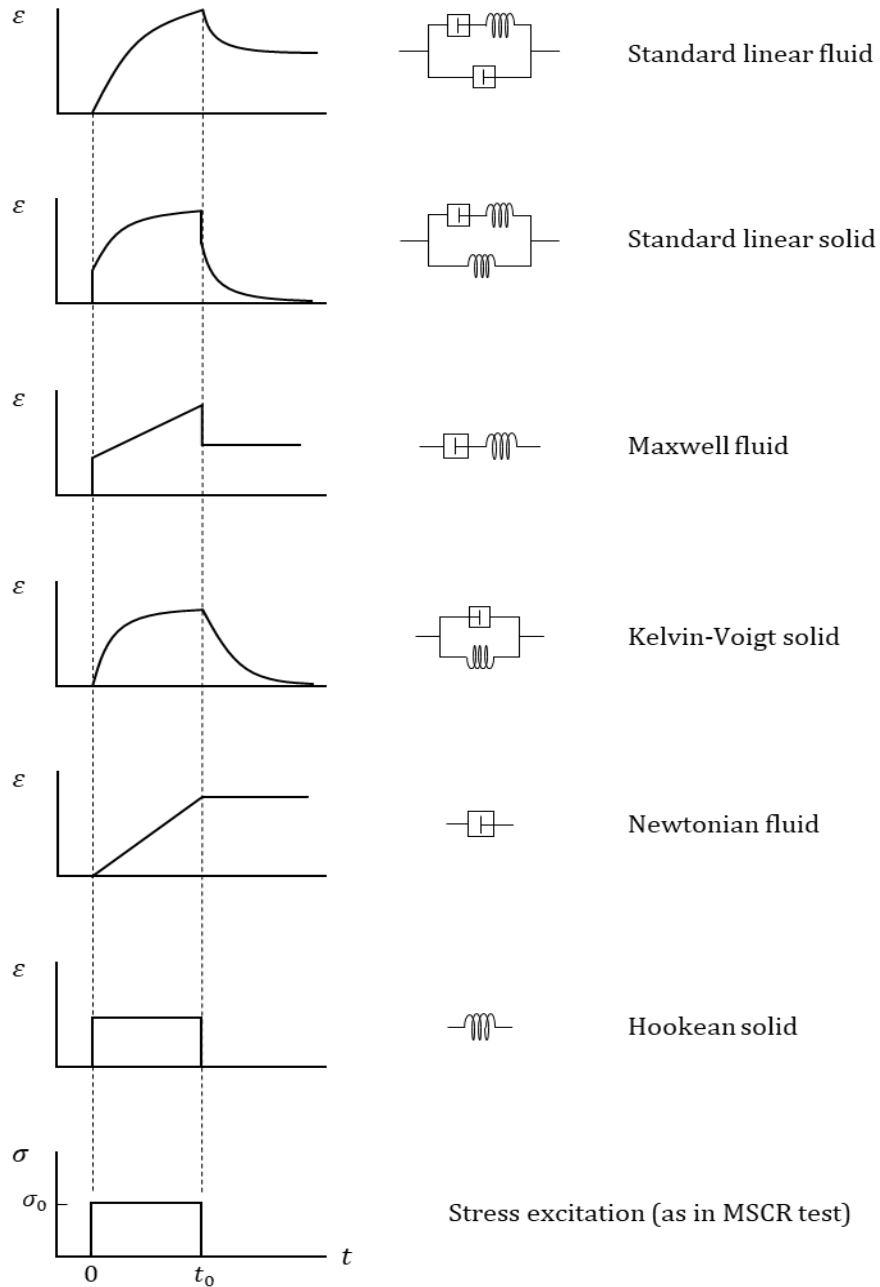
Figure 2.6 Responses of different linear viscoelastic models to MSCR excitation.

The bottom plot in Figure 2.6 shows the applied stress $\sigma(t)$ of a MSCR test. The expected responses of the different rheological model, denoted $\varepsilon(t)$, are illustrated immediately above; all plots share a common time axis. It is clear that the standard linear fluid (Fig. 4b) is the only model that is consistent with empirical observations. *In this thesis, we propose to model asphalt as a standard linear fluid*.

2.2 Predicting Deformation and Flow of Linear Viscoelastic Materials

Thus far, discussions on the deformation/flow of materials have largely been qualitative. We now introduce equations that must be solved to predict, for example, the types of behaviours shown in Figure 2.6. Only *linear* viscoelastic materials will be considered.

2.2.1 Constitutive relations

Constitutive relations provide the connection between the stress σ and the resulting deformation (i.e. the strain ε and its time derivatives) for a given type of material. Two such relations, based purely on empirical observations, have already been introduced; they are for the Hookean solid and the Newtonian fluid (eqn 2.2). From these two fundamental relations — represented metaphorically as springs and dashpots — other linear viscoelastic relations can be derived. When combining springs and dashpots, one needs to apply the following two rules:

- Two elements connected in parallel: They share the same strain, and the overall stress is the sum of the individual stresses.
- Two elements connected in series: They share the same stress, and the overall strain is the sum of the individual strains.

These rules are made more clear in the following sketches:

$$\begin{cases} \sigma = \sigma_A + \sigma_B \\ \varepsilon = \varepsilon_A = \varepsilon_B \end{cases}$$

$$\begin{cases} \sigma = \sigma_A = \sigma_B \\ \varepsilon = \varepsilon_A + \varepsilon_B \end{cases}$$
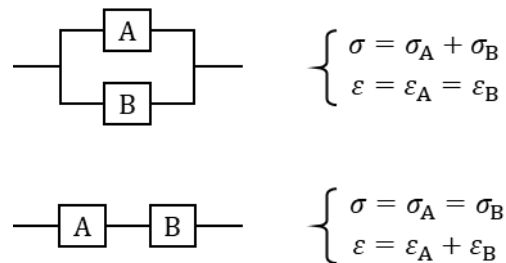
Figure 2.7 Rules for combining two viscoelastic units in parallel and in series.

Straightforward applications of these two rules lead to the constitutive relations listed in Figure 2.8:
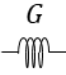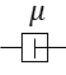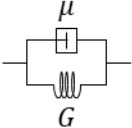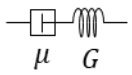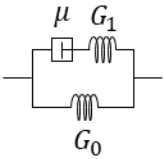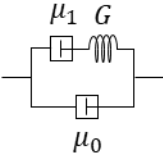
Constitutive relation

Hookean solid	$\overset{G}{-\text{WW}-}$	$\sigma = G\varepsilon$
Newtonian fluid	$\overset{\mu}{-\boxminus-}$	$\sigma = \mu\dot{\varepsilon}$

eqn (2.2)

Kelvin-Voigt solid

$$\sigma = G\varepsilon + \mu\dot{\varepsilon}$$

Maxwell fluid

$$\dot{\varepsilon} = \frac{\dot{\sigma}}{G} + \frac{\sigma}{\mu}$$

Standard linear solid

$$\dot{\varepsilon} = \frac{\dot{\sigma} - G_0\dot{\varepsilon}}{G_1} + \frac{\sigma - G_0\varepsilon}{\mu}$$

Standard linear fluid

$$\dot{\varepsilon} = \frac{\dot{\sigma} - \mu_0\ddot{\varepsilon}}{G} + \frac{\sigma - \mu_0\dot{\varepsilon}}{\mu_1}$$

Figure 2.8 Constitutive relations for some simple linear viscoelastic models.

The last relation in Figure 8, for the standard linear fluid (SLF), is of particular interest since (a) the expression is rarely included in rheology textbooks, and (b) the SLF is identified here as the model for asphalts (§2.1.5). This constitutive relation is rewritten below as a numbered equation:

$$\text{Standard linear fluid:} \qquad \dot{\varepsilon} = \frac{\dot{\sigma} - \mu_0\ddot{\varepsilon}}{G} + \frac{\sigma - \mu_0\dot{\varepsilon}}{\mu_1} \qquad (2.3)$$

where the material properties (μ_0, μ_1, G) are as defined in Figure 2.8.

2.2.2 Solving the constitutive equations

For *linear* viscoelastic models, the constitutive relations are *linear* ordinary differential equations involving $\sigma(t)$ and $\varepsilon(t)$. The general mathematical problem is as follows: given either $\sigma(t)$ or $\varepsilon(t)$, solve for the other function using the appropriate constitutive relation. In this subsection, we consider two situations: (a) The specific case of an SLF that is subjected to MSCR stress excitation (see top and bottom sketches in Figure 2.6), and (b) the general case of having an arbitrary $\sigma(t)$ or $\varepsilon(t)$ as input excitation.

(a) *Standard linear fluid (SLF) subjected to MSCR stress excitation*

Here, the MSCR (multiple stress creep recovery) stress excitation is given by

$$\sigma(t) = \begin{cases} \sigma_0 \; ; & 0 < t < t_0 \\[2mm] 0 \; ; & t > t_0 \end{cases} \tag{2.4}$$

where σ_0 is a constant. This type of excitation is simple enough that an analytical solution can be obtained. Substituting the $\sigma(t)$ from eqn 2.4 into eqn 2.3 (constitutive relation for SLF), one can, after some analysis, arrive at the following:

For $0 < t < t_0^-$

$$\varepsilon(t) = \frac{\sigma_0}{G} \left(\frac{\mu_1}{\mu_0 + \mu_1} \right)^2 [1 - \exp(-t/\tau)] + \left(\frac{\sigma_0}{\mu_0 + \mu_1} \right) t$$

$$\dot{\varepsilon}(t) = \left(\frac{\sigma_0}{\mu_0 + \mu_1} \right) \left[1 + \frac{\mu_1}{\mu_0} \exp\left(-\frac{t}{\tau} \right) \right] \tag{2.5}$$

where

$$\tau \equiv \frac{\mu}{G}, \quad \text{with} \quad \frac{1}{\mu} \equiv \frac{1}{\mu_0} + \frac{1}{\mu_1} \quad \text{or} \quad \mu = \frac{\mu_0 \mu_1}{\mu_0 + \mu_1} \tag{2.6}$$

From these equations, three quantities are evaluated at $t = t_0^-$:

$$\left. \begin{array}{l} \varepsilon(t_0^-) = \cdots \\[3mm] \dot{\varepsilon}(t_0^-) = \cdots \end{array} \right\} \text{using eqns 2.5}$$

and

$$\varepsilon_e(t_0^-) = \frac{\sigma_0 - \mu_0 \dot{\varepsilon}(t_0^-)}{G} \quad \text{(strain of the elastic element)}$$

23

<u>For $t > t_0^+$</u>

$$\varepsilon(t) = \varepsilon(t_0^-) - \varepsilon_r \left[1 - \exp\left(-\frac{t - t_0}{\tau}\right) \right] \tag{2.7}$$

where

$$\varepsilon_r = \left(\frac{\mu_1}{\mu_0 + \mu_1}\right) \varepsilon_e(t_0^-)$$

is the recoil in strain.

(b) *General problem of arbitrary excitation*

In this general case, the input excitation is some prescribed $\sigma(t)$ or $\varepsilon(t)$; the response [the other function — either $\sigma(t)$ or $\varepsilon(t)$] is obtained by solving the appropriate constitutive relation which, in mathematical terms, is a linear ordinary differential equation (ODE).

It is always possible to solve ODEs numerically. For analytical solutions, the best approach is perhaps to make use of integral transforms (e.g. Laplace or Fourier transform) that take the problem from the time domain to the complex or frequency domain. The advantage of using integral transforms is that linear ODEs in the time domain are converted to algebraic equations in the complex/frequency domain, where they can be handled much more easily. The Laplace transform is suitable for transient problems with prescribed initial conditions, while the Fourier transform is ideal for periodic excitations with the response having already reached steady state.

2.2.3 The dynamic modulus

We now focus on a special case in which (a) the excitation (either σ or ε) is a *sinusoidal* function of time, and (b) the response has reached steady state. At steady state, both the excitation and the response are sinusoidal functions *at the same frequency*; there is, however, a phase difference between the two waveforms. Without loss of generality, we will assume the excitation to be an imposed strain that is a sine (or cosine) function with magnitude ε_0 and frequency ω; the resulting stress will also be a sine (or cosine) function as expressed in eqn 2.8:

$$\varepsilon(t) = \begin{cases} \varepsilon_0 \sin \omega t \\ \text{or} \\ \varepsilon_0 \cos \omega t \end{cases} \Rightarrow \quad \sigma(t) = \begin{cases} \sigma_0 \sin(\omega t + \delta) \\ \text{or} \\ \sigma_0 \cos(\omega t + \delta) \end{cases} \tag{2.8}$$

Here, σ_0 is the stress amplitude and δ the phase difference. For a linear viscoelastic material, the following two features are important to note:

- At a given frequency ω, the ratio σ_0/ε_0 is constant, regardless of the value of ε_0.
- Both σ_0/ε_0 and δ are functions of ω.

The problem now is to determine how σ_0/ε_0 and δ vary as functions of ω. In principle, this can be done by substituting the expressions for $\varepsilon(t)$ and $\sigma(t)$, as given in eqn 2.8, into the appropriate constitutive relation (for example, eqn 2.3) and solving for σ_0/ε_0 and δ. Unfortunately, for such a process, the algebra can quickly become unwieldy.

A much easier way of tackling the same problem is to make use of Euler's formula

$$e^{i\theta} = \cos\theta + i\sin\theta$$

and rewrite eqn 2.8 as

$$\varepsilon(t) = \varepsilon_0\, e^{i\omega t} \quad \Rightarrow \quad \sigma(t) = \sigma_0\, e^{i(\omega t + \delta)} \tag{2.9}$$

where the real part of $e^{i\omega t}$ is understood to represent $\cos\omega t$, and the imaginary part $\sin\omega t$. The expressions in eqn 2.9 can now be substituted into the relevant constitutive relation, and the quantities σ_0/ε_0 and δ are determined as functions of ω. This approach of exploiting Euler's formula is similar to the use of Fourier transform in that a linear ODE in time t — the constitutive relation — is converted into an algebraic equation with the frequency ω being the new independent variable (after cancelling the common factor of $e^{i\omega t}$ from all terms).

Once the functions $\sigma_0/\varepsilon_0(\omega)$ and $\delta(\omega)$ are known, the problem is considered completely solved. It is conventional, however, to introduce yet another quantity called the *dynamic modulus*, denoted G^*, such that

$$G^* \equiv \sigma(t)/\varepsilon(t) \tag{2.10}$$

Combining this with the expressions in eqn 2.9, we have

$$G^* = \frac{\sigma_0}{\varepsilon_0}\, e^{i\delta} \tag{2.11}$$

From the above expressions, two important observations are made:

- It is clear from eqn 2.11 that G^* is a complex quantity (while noting that σ_0 and ε_0 are real numbers).

- The time-dependent factor $e^{i\omega t}$, which appears in both $\sigma(t)$ and $\varepsilon(t)$, is cancelled out when the stress is divided by the strain, leaving G^* as a function of only the frequency ω (since, as noted earlier, both σ_0/ε_0 and δ depend on ω).

Next, we define $G'(\omega)$ and $G''(\omega)$ as the real and imaginary parts of $G^*(\omega)$, i.e.

$$G^*(\omega) \equiv G'(\omega) + iG''(\omega) \tag{2.12}$$

From eqn 2.11, it is clear that

$$G' = \frac{\sigma_0}{\varepsilon_0}\cos\delta \; ; \quad G'' = \frac{\sigma_0}{\varepsilon_0}\sin\delta \tag{2.13}$$

It also follows that

$$\frac{\sigma_0}{\varepsilon_0} = |G^*| = \sqrt{(G')^2 + (G'')^2} \; ; \quad \tan\delta = \frac{G''}{G'} \tag{2.14}$$

Finally, by combining eqns 2.8 and 2.13, one can write

$$\sigma = G'\varepsilon + \frac{G''}{\omega}\dot{\varepsilon}$$

Comparing this with the Hookean and Newtonian expressions in eqn 2.2, it appears that G' plays the role of an elastic modulus, while G''/ω is an effective viscosity. For these reasons, the quantity G' is often called the "storage modulus" (similar to the way an elastic spring stores and releases mechanical energy without dissipation), and G'' is called the "loss modulus" (referring to the loss of mechanical work to heat through internal friction). However, it should be noted that $G'(\omega)$ and $G''(\omega)$ are *not* true material properties, as their values will change with the excitation frequency (i.e. they depend on the experimental conditions).

Thus far, all equations in §2.2.3 are general, i.e. they are used to describe *any* linear viscoelastic material (for example, any of the six cases in Figure 2.8). We now focus on the standard linear fluid (SLF): its material properties are defined in the following sketch:

μ_1 G

Standard linear fluid

μ_0

and its constitutive relation is given by eqn 2.3. From this equation, it is straightforward to arrive at the dynamic modulus using complex variables; the results are as follows:

$$\left.\begin{array}{l} \dfrac{G'(\omega)}{G} = \dfrac{(\tau_1\omega)^2}{1+(\tau_1\omega)^2} \\[4mm] \dfrac{G''(\omega)}{G} = \dfrac{\tau_0\omega\left[1+(\tau_1\omega)^2\right]+\tau_1\omega}{1+(\tau_1\omega)^2} \end{array}\right\} \quad \text{SLF} \qquad (2.15)$$

where

$$\tau_0 \equiv \mu_0/G \;;\quad \tau_1 \equiv \mu_1/G \qquad (2.16)$$

It is also possible to combine the two expressions in eqn 2.15 and get

$$\frac{G''}{\omega} = \frac{G}{\mu_1}\frac{G'}{\omega^2}+\mu_0 \qquad (2.17)$$

From these equations, one can obtain the SLF material properties (i.e. G, μ_0 and μ_1) using the following procedures:

1. Determine, from experiments, $G'(\omega)$ and $G''(\omega)$.

2. Plot G'' vs ω. The slope at the origin should give $\mu_0+\mu_1$ (based on the second of eqns 2.15). This is sometimes called the "zero-frequency viscosity."

3. Plot G''/ω vs G'/ω^2. If the material is truly linear viscoelastic, the plot should be a straight line (according to eqn 2.17). The y-intercept should give μ_0, while G can be determined from the slope.

2.3 Other Viscoelastic Models for Asphalt

2.3.1 Study of asphalt rheology: Two general approaches

There is no question that asphalts behave as viscous fluids. As the constituent molecules of asphalts are fairly large ($\sim 10^3$ Da), the material is generally non-Newtonian. If one assumes, as is often done, that asphalt is linearly viscoelastic, it is natural to characterize the material through measurements of G' and G'' at different frequencies. Due to experimental limitations, empirical data of $G'(\omega)$ and $G''(\omega)$ can only be obtained over a limited range of frequencies; however, it is relatively easy to repeat such experiments at different temperatures. In the past decades, there had been two lines of activities aimed at delineating the rheological properties of asphalt:

(i) Linear viscoelastic models were proposed ([22] [23]), leading ultimately to expressions for $G^*(\omega)$ [i.e. $G'(\omega)$ and $G''(\omega)$]. Model parameters are obtained by fitting theory to empirical data.

(ii) Based on the principle of *time-temperature superposition* ([24] [25]), rheological data obtained at different temperatures are combined to form a single plot of G^* (or some other rheological parameter) vs ω over an *extrapolated* frequency range — one that is far wider than what is attainable experimentally. This is done with the belief that

$$\underbrace{G^*(\omega) \text{ at } T}_{\text{experimental}} \; = \; \underbrace{G^*(a_T\omega) \text{ at } T_{\text{ref}}}_{\substack{\text{time-temperature} \\ \text{superposition}}}$$

where T_{ref} is some reference temperature, and a_T is a dimensionless shift factor that depends on T and T_{ref} through some empirical relation. The resulting $G^*(a_T\omega)$, often called the "master curve," depicts rheological properties at temperature T_{ref} over an extremely wide range of extrapolated (or "reduced") frequencies $a_T\omega$.

These two lines of activities are essentially independent of one another: "master curves" can be assembled regardless of the validity of the rheological model(s). In this thesis, we focus only on the first activity, namely, introduction of an appropriate rheological model for asphalts. We choose not to construct master curves since, as is commonly known in polymer physics, the principle of time-temperature superposition is valid only for "thermorheologically simple" fluids (ideally those composed of linear and monodisperse polymers). In the context of *relaxation times*, which will be discussed further in the next

section, time-temperature superposition applies only when all relaxation modes within a material have the same temperature dependence [24]. In situations, such as with asphalts, where the molecules have a wide variety of molecular weights and chemical structures (e.g. branched polymers, block copolymers, etc.), the relaxation modes are certain to have different temperature dependencies, and application of the superposition principle would therefore not be justified.

2.3.2 Stress relaxation

Consider a material that is subjected to a step increase in strain, resulting in a sudden jump in stress within the body. (Whether the material can undergo abrupt deformation will be discussed in the next section.) For some materials, stresses created by deformation can decrease — or "relax" — spontaneously over time *while maintaining the same level of strain*; such a process is called stress relaxation. (For polymeric materials, this can be due to the extension and subsequent recoil of the macromolecules.) The simplest mechanical model for stress relaxation is the Maxwell fluid — first illustrated in Fig. 2.3, and shown again below in Figure 2.9:
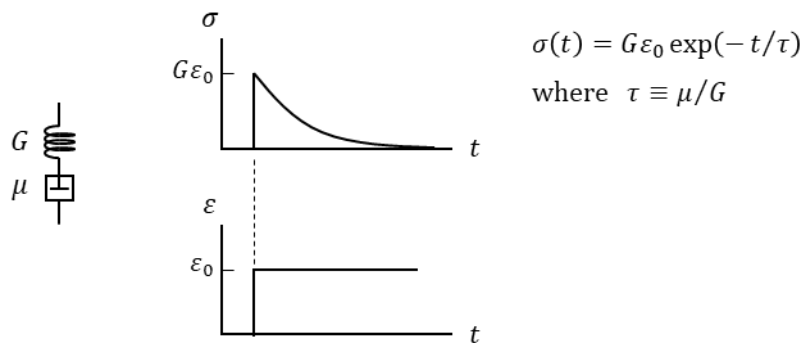

Figure 2.9 Stress relaxation of a Maxwell fluid.

As shown in Figure 2.9, the stress relaxation of a Maxwell fluid, in response to a step strain of magnitude ε_0, is

$$\sigma(t) = G\varepsilon_0 \exp(-t/\tau) \tag{2.18}$$

where $\tau \equiv \mu/G$ is the characteristic time of relaxation.

For materials with multiple relaxation times, the "generalized Maxwell model" (GMM), which is simply a number of Maxwell fluids connected in parallel, is often put forward to represent the underlying rheology. An illustration of the GMM is shown in Figure 2.10:
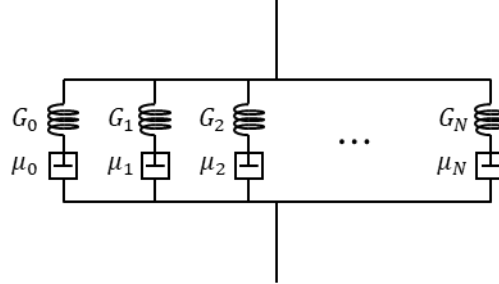
Figure 2.10 The generalized Maxwell model (GMM) comprises a number of Maxwell fluids connected in parallel.

Since the Maxwell fluids in a GMM are arranged in parallel, the resulting stress is just the sum of the individual relaxations:

$$\text{GMM:} \quad \sigma(t) = \sum_{i=0}^{N} G_i \varepsilon_0 \exp(-t/\tau_i); \quad \tau_i \equiv \mu_i/G_i \tag{2.19}$$

It is also customary to define the *relaxation modulus $R(t)$* as

$$R(t) \equiv \sigma(t)/\varepsilon_0 \tag{2.20}$$

which is simply the transient stress in a material in response to unit step strain. From eqn 2.19, the relaxation modulus of the GMM is

$$R(t) = \sum_{i=0}^{N} G_i \exp(-t/\tau_i) \tag{2.21}$$

where $(\tau_0, \tau_1, \cdots \tau_N)$ are the relaxation times.

Continuous distribution of relaxation times

Equation 2.21 represents materials with *discrete* sets of relaxation times. If the τ_i's are spaced so closely together that they effectively form a continuous distribution, one can imagine (a) the number of relaxation modes, N, will approach infinity, and (b) the elastic

moduli and viscosities will become incremental — and eventually, differential — quantities, while their ratios $\tau_i = \Delta\mu_i/\Delta G_i$ remain finite. In such a limit, the sum in (2.21) can be expressed as an integral as follows:

$$R(t) = \lim_{N\to\infty} \sum_{i=0}^{N} \Delta G_i \exp(-t/\tau_i) = \int_{\tau=0}^{\infty} dG(\tau) \cdot \exp(-t/\tau)$$

In the literature, it is common to write

$$dG(\tau) \equiv H(\tau)\frac{d\tau}{\tau} \tag{2.22}$$

where $H(\tau)$, with units of Pa, is called the *relaxation spectrum*. With this, the relaxation modulus $R(t)$ now becomes

$$R(t) = \int_{0}^{\infty} H(\tau) \exp(-t/\tau)\,\frac{d\tau}{\tau} \tag{2.23}$$

Note that there is no fundamental physics behind eqn 2.22; it is simply a *definition* of the relaxation spectrum $H(\tau)$. [Some authors may choose to write $dG \equiv H(\tau)\,d\tau$, in which case H would have units of Pa/s.]

Before proceeding to the next section, we digress slightly and introduce two additional equations: The total elastic and viscous moduli of the GMM, in the limit of a continuous distribution of relaxation times, are

$$G_{\text{tot}} = \lim_{N\to\infty} \sum_{i=0}^{N} \Delta G_i = \int_{\tau=0}^{\infty} dG(\tau)$$

$$\mu_{\text{tot}} = \lim_{N\to\infty} \sum_{i=0}^{N} \Delta\mu_i = \lim_{N\to\infty} \sum_{i=0}^{N} \tau_i \Delta G_i = \int_{\tau=0}^{\infty} \tau\,dG(\tau)$$

Combining these expressions with eqn 2.22, we can relate G_{tot} and μ_{tot} to the relaxation spectrum $H(\tau)$ as follows:

$$G_{\text{tot}} = \int_0^\infty \frac{H(\tau)}{\tau} \, d\tau \tag{2.24}$$

$$\mu_{\text{tot}} = \int_0^\infty H(\tau) \, d\tau \tag{2.25}$$

2.3.3 Viscous fluids that cannot deform instantaneously

When subjected to a sudden increase in stress, most viscous fluids — including asphalts — are incapable of responding with instantaneous deformation. To model such fluids using mechanical analogues (i.e. with springs and dashpots), one necessary requirement is that there must be *one dashpot that directly connects one end of the mechanical model to the other end*. Turning now to the generalized Maxwell model in Figure 10: if one insists on applying the GMM to fluids that cannot deform instantaneously, one of the Maxwell fluid elements — say the first one — must provide the "end-to-end dashpot"; it follows that the elastic spring of that Maxwell fluid should be infinitely stiff, i.e.

$$G_0 = \infty \quad \Rightarrow \quad \tau_0 = \mu_0/G_0 = 0$$

With these simple arguments, one can infer the following:

- *The case of discrete relaxation times*
  One of the relaxation times must be zero. That Maxwell fluid element, with $\tau = 0$, must have an infinitely stiff spring which allows the viscous dashpot to prevent any sudden jump in strain.

- *The case of a continuous distribution of relaxation times*
  The value of $H(\tau)$ must be infinite at $\tau = 0$ (this is analogous to infinite stiffness in the discrete case). It is noted that, as evident from eqn 2.25, any "infinity" on the relaxation spectrum must be integrable (for the material to be a viscous fluid). If the proposed $H(\tau)$ is "well behaved" away from $\tau = 0$, then the spectrum must include a Dirac delta function, of magnitude μ_0, at the vertical axis (see Figure 2.11). In such a case, the total viscosity of the GMM (from eqn 2.25) is

$$\mu_{\text{tot}} = \mu_0 + \int_{0^+}^\infty H(\tau) \, d\tau$$
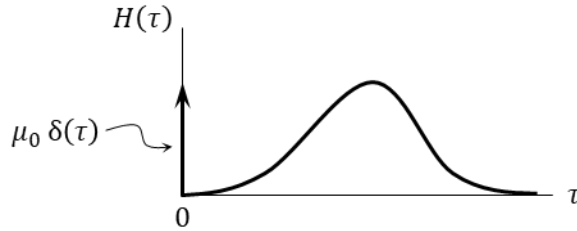
Figure 2.11 For a relaxation spectrum that is "well behaved" away from $\tau = 0$, one must include an impulse function at $\tau = 0$ to prevent instantaneous deformation of the fluid under a sudden increase in stress.

Recall from §2.1.5 that, in this thesis, we are proposing to use the standard linear fluid (SLF) as the model for asphalt. In terms of the parameters defined earlier, the SLF has two *discrete* relaxation times: 0 and μ_1/G. This, we believe, is the model of minimal complexity that captures the essential physics of asphalts — and indeed, of any viscous fluid that (a) does not deform instantaneously, and (b) is so inhomogeneous and varied in composition that the relaxation spectrum cannot be unique, and stress relaxation is best described by a single, effective characteristic time.

2.3.4 Two common viscoelastic models for asphalt

A number of viscoelastic models for asphalt have appeared in the literature. Here, we briefly mention two models that are perhaps the most invoked and explain why we feel the need to introduce yet another alternative.

The 2S2P1D model

2S2P1D stands for "two springs, two parabolic elements, and one dashpot" ([26], [27], [28]). A schematic of the model is shown in Figure 2.12.

Figure 2.12 The 2S2P1D model for asphalt. The two elements labelled "P" are the so-called parabolic elements.

The 2S2P1D model is an extension of its predecessor, the Huet-Sayegh model, which did not include the dashpot. The parabolic element is itself a "mini-rheological model" involving several adjustable parameters and depends on the frequency of excitation.
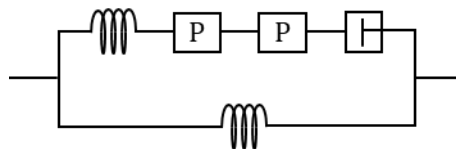
It is not important here to examine the details of the parabolic element. We choose not to adopt the 2S2P1D model (nor the Huet-Sayegh model) for asphalt for one simple reason: it is clear that both these models predict instantaneous deformation when the material is subjected to a step increase in stress (no dashpot *directly* connecting one end of the model to the other).

The Christensen-Anderson model

In this model, "relaxation spectra of asphalt binders" are assumed to follow "a skewed logistic distribution function"([29], [30]) . Presumably, the "relaxation spectra" are $H(\tau)$ as defined in eqn 2.22 — although this is unclear (see Point 2 below). The "skewed logistic distribution function" is simply a probability distribution, like the "bell curve," that is skewed to one side. It is also not clear why such a probability distribution was chosen for this purpose. The magnitude of the resulting dynamic modulus is

$$|G^*(\omega)| = G_g \left[1 + \left(\frac{\omega_c}{\omega}\right)^{\log 2/R}\right]^{-R/\log 2} \tag{2.26}$$

where G_g, ω_c and R are, respectively, the glassy modulus, the crossover frequency, and the rheological index (i.e. they are the three model parameters). Here, we choose not to adopt such a model for asphalt for two reasons:

- According to the model, the value of $H(\tau)$ at $\tau = 0$ is zero (see eqn 13 in [30]). This, as we argued above, implies that asphalt is capable of instantaneous deformation under a step increase in stress. This contradicts empirical observation.

- The logical developments, which began with the skewed logistic function and ended with eqn 2.26, have completely escaped us (see §5.1 in [29]).

Chapter 3: Materials and Experimental Methods

The experiments performed in this research were conducted at Gecan in Acheson, Alberta. (Gecan is one of the largest asphalt testing facilities in Canada, with plenty of state-of-the-art equipment and machinery.) The asphalt binders used in this study were provided by the McAsphalt Industries Ltd. terminal based in Acheson. The following sections outline how the asphalt binders used in this study were collected, prepared and evaluated.

3.1 Materials

To differentiate between asphalt samples, they are referred to by their PG designations – previously described in Chapter 1. It is noted here that none of the binders were verified to meet PG specifications in this study. However, these materials are tested and sold year-round and can be assumed to meet PG specifications. Additionally, as the aim of this thesis is to introduce a rheological model and its functionality – as opposed to comparing the model's ability to predict road performance – it is enough to know that the samples being tested are considered to be sufficiently distinct under the PG system. Between the 6 samples, 3 are unmodified and 3 are polymer modified asphalts.

The unmodified grades are PG 46-34, PG 58-28, and PG 64-22, while the modified grades are PG 58-37P, PG 64-34P, and PG 70-31P. Grades with different and identical high temperature limits are chosen to easily identify trends and changes in the resulting SLF model parameters. Furthermore, the PG 58-28 is the basis for the PG 70-31P, which allows for straightforward identification of the polymer's effects on the model parameters. The polymer used was styrene-butadiene copolymers. As the formulations of these asphalt binders is proprietary information, the specific quantity of polymer addition is not known, but the amount can range from 1-10% by weight for polymer modified grades.

At McAsphalt's Acheson terminal, all the asphalt binders are mixed in large, heated storage tanks. From the large storage tanks, small batches are released into 5-gallon pails. These pails were heated in a 163°C oven until homogenous, then poured into pint cans for easier handling and reduced re-heating time.

3.2 Equipment and Software

The only piece of measuring equipment used in this study is the aforementioned DSR, or Dynamic Shear Rheometer. The specific make and model are: TA Instruments, Discovery HR-1 (Hybrid Rheometer). This hybrid rheometer can operate in either controlled stress or controlled strain mode. The DSR uses Upper Heated Plate technology to ensure that there are no vertical temperature gradients through the sample. The geometry used was 25mm in diameter, stepped, stainless steel Pelletier plates. with the lower plate being fixed while the upper plate is free to rotate. The software used to record data throughout the experiments is TA Instruments TRIOS Version 5.0.0. Figure 3.1 depicts the HR-1 and Pelletier plates.

Figure 3.1 Discovery HR-1 Rheometer and Pelletier plates [31].

3.3 Procedures

3.3.1 Conditioning

The small pint cans were placed in an oven set at 163°C until the sample was homogenous and fluid. This process typically takes 1 hour, when stirring the sample every 15 minutes after half an hour has passed. Polymer-modified grades may take up to 1.5 hours with this method. Next, a sample is poured from the pint can onto a silicone mold (25mm diameter) and allowed to cool until the binder can detached from the mold. The sample is then loaded onto the bottom plate of the DSR (preheated to 58°C) and allowed to condition for 1-2 minutes. The top plate is then set to the trim height, 1050 microns, and trimmed using a heated metal spatula until the sample is flush with the plates. Next, the top plate is set to the desired gap height, 1000 microns, and allowed to condition undisturbed for 10 minutes.

Using TRIOS, a pre-shear rate of 1.0 (1/s) was applied for 30 seconds before another 5 minutes of undisturbed conditioning. Pre-shearing serves to standardize the loading procedure and ensure all samples have the same initial state. The sample is now conditioned, and the desired experiment can be performed. It is noted here that for all samples, the experiments were performed at 58°C.

3.3.2 Frequency Sweep

With TRIOS, frequency sweeps were performed between 10 - 80 rad/s, at stress levels of 1, 10 and 100 Pa. To facilitate data collection, the experiment was performed using the "Oscillation – Amplitude" input rather than the "Oscillation – Frequency" input. The "discrete sweep" option in Amplitude mode allows for repeated points. For each stress, six data points were collected per angular frequency. The default data acquisition settings of 3 seconds of conditioning and sampling time, and 64 points per waveform were used. No other additional options were changed or enabled. Before moving on to the next stress level (but not between angular frequency increases), the pre-shearing and 5-minute equilibration time were applied to the sample again. An average value was then calculated for the G', G'', and $\tan\delta$ values at each frequency.

3.3.3 MSCR Variation

Using TRIOS, a modified version of the MSCR procedure (as described in section 2.2.2) was created. In this pulse version, the creep loading is applied for 1 second (as standard MSCR procedure) but an indefinite amount of recovery time is allowed. There are no further cycles of stress on and off the binder. The experiment is performed using the "Step Transient – Repeated Creep" input. With this input, the software automatically enforces a data collection rate that is initially very fast, but gradually slows down exponentially. To mimic current MSCR protocol, two stress levels are used, 100 Pa and 3200 Pa. The software caps allowed recovery time to 1000 seconds, but in some data sets the procedure was manually ended before this time had reached, as there was clearly no further recovery. The samples were pre-sheared and allowed to equilibrate before each stress level. Due to the large time scales difference between the creep and recovery portions, the data is split into two sections. This allows for an easier interpretation of their individual effects.

Chapter 4: Results and Discussion

Appendix A contains the frequency sweep data and MSCR pulse responses. An example of obtaining the SLF parameters and the Matlab code template are included in Appendix B.

4.1 Frequency Sweep Results

"Frequency sweeps" are experimental determination of how rheological parameters — in this case, the phase angle δ — vary with the excitation frequency ω. Figure 4.1 shows $\tan \delta$ vs ω at the stress amplitudes of 1, 10 and 100 Pa for asphalt binder PG 58-28. This data was acquired as outlined in §3.3.2. At the lower frequencies, there is a small discrepancy in $\tan \delta$ between small and large stresses. As the frequency increases, the discrepancy is reduced. This trend exists for all binders. In general, the variation between the 6 data points collected per frequency, per stress, was highest at smaller stresses and frequencies. This is likely due to low torque (or stress) values being less controlled when shearing the material. Below 1 Pa of stress, the minimum torque limit of the DSR needs to be considered. The variation was negligible for 100 Pa data at all frequencies. Regardless, the value of $\tan \delta$ does not change significantly with stress, which is indicative of a linear viscoelastic material. As the 100 Pa data is the most reliable, it is used in subsequent analysis.
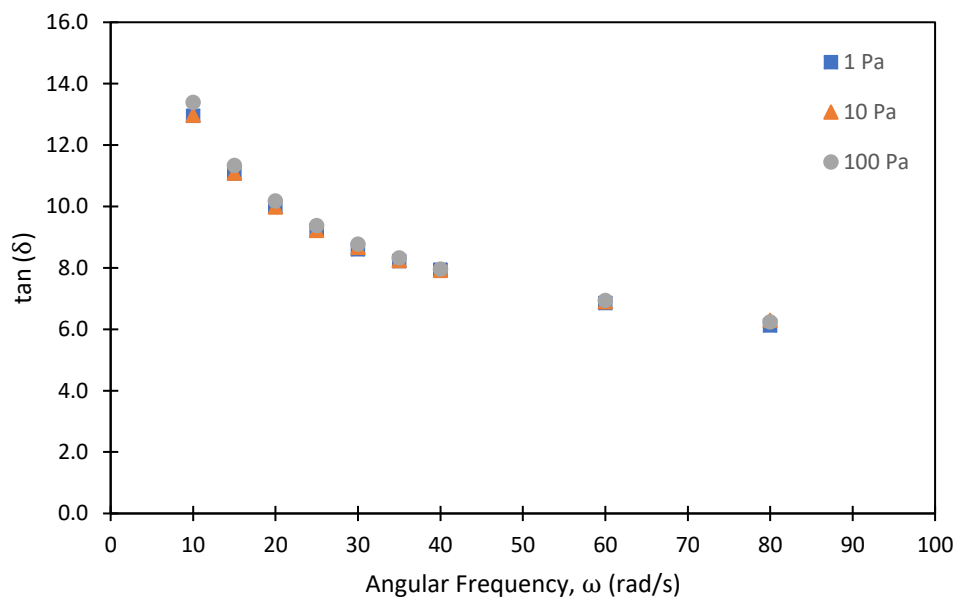

Figure 4.1 $\tan \delta$ vs ω, for PG 58-28 at 1, 10, and 100 Pa stresses.

Figure 4.2 shows the frequency sweep data at 100 Pa for the unmodified and polymer-modified binders. For the unmodified binders (grades that do not end with a "P"), there is a difference in tan δ of at least 5 between low and high frequency results. Initially, the value of tan δ is dropping at a steep rate. At 30 rad/s the rate continues to decrease but is less sharp. By 80 rad/s, the decrease in tan δ has begun to flatten out. Between unmodified binders, the difference in tan δ is significant. This is in stark contrast to the polymer modified binders (those grades whose designations end with a "P" — a reminder that they are polymer-modified). These modified binders show very little difference from each other. The range of tan δ values are much smaller, only decreasing from 3 to 2 over the sweep range. Smaller tan δ indicates a stronger elastic presence (recall eqn 2.14), which is to be expected with the addition of polymer to these binders. Additionally, the decrease of tan δ with frequency appears linear. This suggests the viscous and elastic moduli are changing by comparable amounts with frequency. For the unmodified binders, they behave more like viscous fluids (i.e. larger tan δ) at lower frequencies, as expected. Interestingly, at high frequencies, PG 46-34 became indistinguishable from the polymer modified binders. A deeper look into the storage and elastic modulus values seems necessary to find out if there are truly any similarities between these materials.
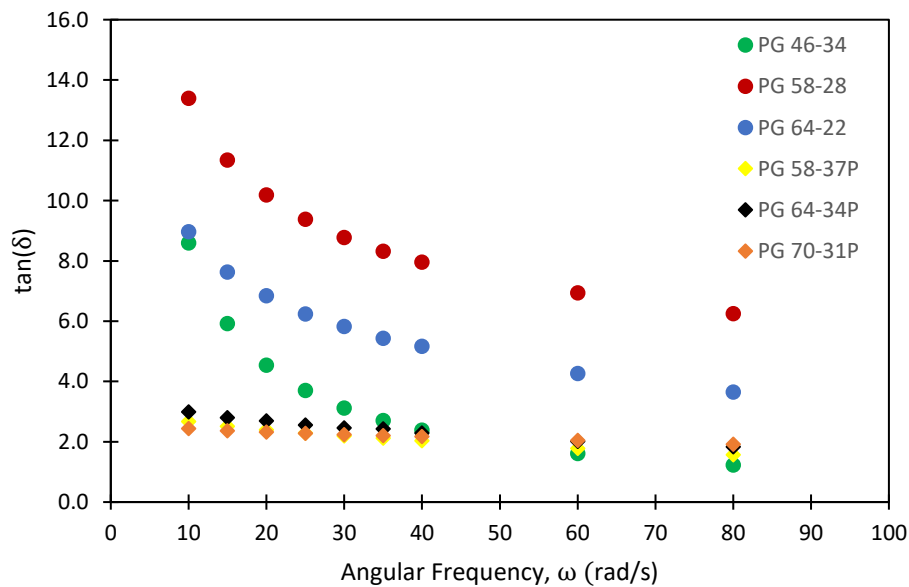

Figure 4.2 tan δ vs ω, for unmodified and modified binders at 100 Pa.

Figure 4.3 shows the storage modulus G' as a function of angular frequency for PG 46-34 and PG 58-37P, at 100 Pa. For both binders, G' increases with ω. At low frequencies, the storage modulus is essentially non-existent for the PG 46-34 binder. As the frequency is increased, a quadratic relationship is evident. However, even at the highest frequencies, the values of G' are not comparable to those of PG 58-37P. The addition of polymer has increased the storage modulus significantly at all frequencies. Moreover, the rate of increase of the storage modulus appears not quadratic, but linear. Based on Figure 4.3, it is clear that the PG 46-34 and PG 58-37P binders are rheologically distinct.
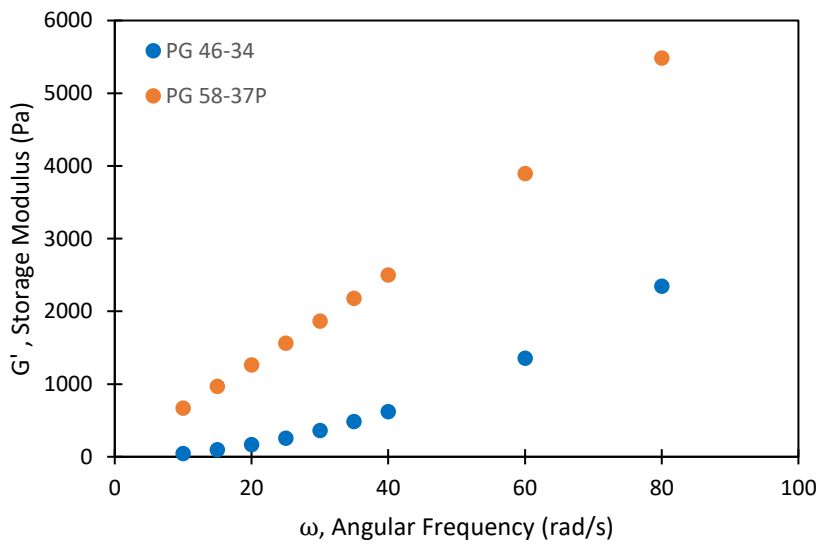
Figure 4.3 G' vs ω for PG 46-34 and PG 58-37P.

Figure 4.4 shows the loss modulus G'' as a function of the angular frequency ω for PG 46-34 and PG 58-37P, at 100 Pa. In both cases, G'' increases with ω, just as G' did. However, in this dataset, there is clearly a linear trend for the PG 46-34. A linear relationship for G'' through the origin is equivalent to a Newtonian fluid (§2.2.3). As with the storage modulus, the addition of polymer has greatly increased the loss modulus at all frequencies for PG 58-37P. In addition, the polymer also seems to have caused the loss modulus to develop a slight shear-thinning trend. Again, there are no rheological similarities between the PG 46-34 and PG 58-37P binders. Instead, we have seen that the unmodified material is linear in viscosity, while the polymer modified is linear in elasticity.
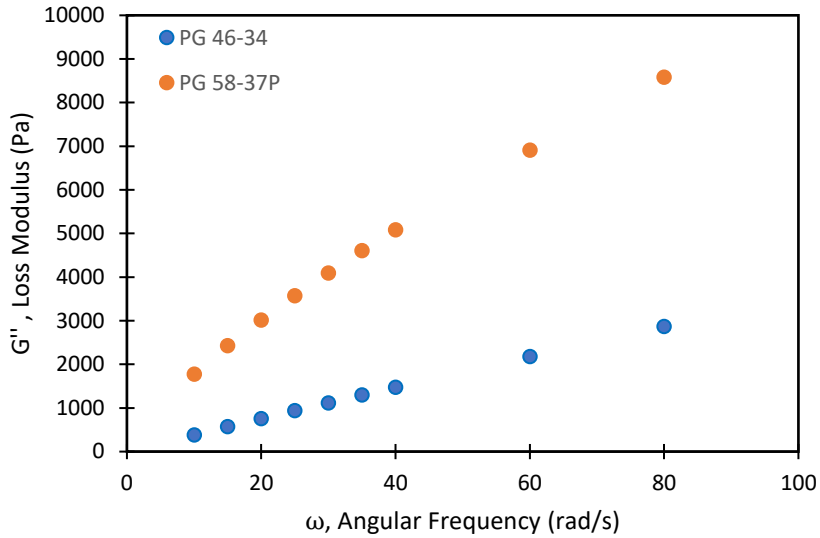
Figure 4.4 G'' vs ω for PG 46-34 and PG 58-37P.

Despite what the results of Figure 4.2 suggest, it is clear that PG 46-34 and PG 58-37P are quite different from each other, even at high frequencies. They do not share viscous or elastic characteristics. Without looking deeper into the data, incorrect conclusions could be made. Looking at the other frequency sweep results, it is worth asking what other inconsistencies could be embedded in the tan δ vs ω data? For example, why are the responses different between unmodified binders? Are polymer-modified binders indistinguishable from each other?

Although it is relatively simple to repeat these experiments, it is not always clear what the significance of the storage and loss modulus are. Recall from §2.2.3 that they are not truly material properties, but parameters dependent on the experimental conditions. Hence, it is possible that materials with entirely different viscoelastic behavior can appear similar. The purpose of the storage and loss modulus is to summarize viscoelastic behavior. However, there is obviously a risk in utilizing these parameters at only one frequency (as the PG system does). A much better approach of measuring material properties would include an evaluation of their fundamental engineering parameters. By fitting the range of $G'(\omega)$ and $G''(\omega)$ data to the Standard Linear Fluid model, that can be achieved.

41

4.2 Standard Linear Fluid Model

4.2.1 Fitting SLF Model

As outlined in Chapter 2, the material properties in the SLF model can be found from $G'(\omega)$ and $G''(\omega)$ data. First, the total viscous contributions are determined from the slope of the $G''(\omega)$ data. Figure 4.5 shows a modified version of Figure 4.4, with a linear trendline fit through the origin using the two slowest frequency points. The slowest points provide a better estimate of the zero-frequency viscosity than a trendline that uses high frequency data. Trendlines are fit using the built-in trendline option in Excel. From this figure, we can deduce that $(\mu_0 + \mu_1) = 38.075$ Pa-s for PG 46-34.
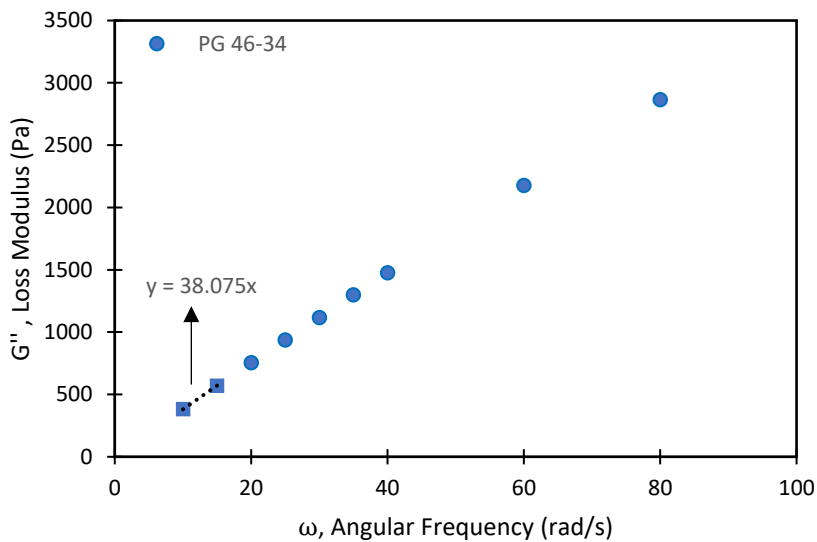
Figure 4.5 Solving for $(\mu_0 + \mu_1)$ of PG 46-34.

Next, a plot of G''/ω vs G'/ω^2 is created to obtain the material properties. As mentioned in Chapter 2, according to eqn (2.17), the plot should be a straight line with the y-intercept giving μ_0, while G can be determined from the slope. Figure 4.6 shows G''/ω vs G'/ω^2 for PG 46-34, with ω ranging from 10 to 80 rad/s at 100 Pa. Again, a linear trendline is fit (*not* through the origin) using Excel. From this plot, it is evident that the material does not fit linearly through the range of frequencies. At the lowest values of G'/ω^2 (highest frequencies) the data begins to divert from linearity. Although the fit is not terrible ($R^2 = 0.9411$), the trendline is negatively influenced by the high frequency data points. It is worth pointing out

that this trend existed for all data sets, whether the binder is unmodified or polymer-modified.
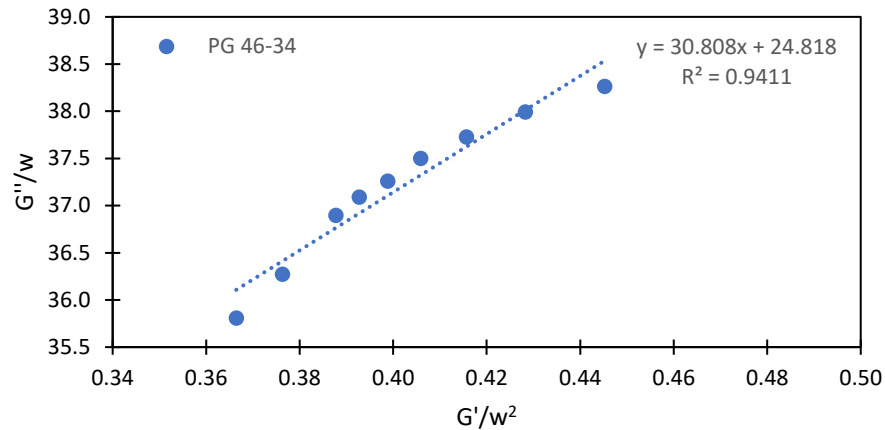
Figure 4.6 Full range (10-80 rad/s) of G''/ω vs G'/ω^2 for PG 46-34 at 100 Pa

Figure 4.7 shows a modified version of Figure 4.6, with the highest frequency data (60 and 80 rad/s) removed. In this plot, the trendline fit is noticeably better ($R^2 = 0.9785$). None of the points deviate from the trendline significantly, and the data reasonably resembles a straight line. This frequency range offers the most information without compromising the necessity that the relationship is linear. Thus, the SLF material properties are deduced using the 10–40 rad/s data.
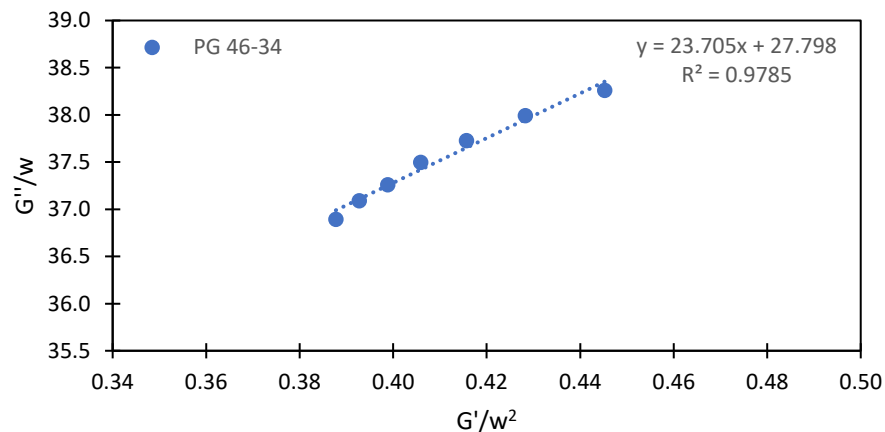
Figure 4.7 Modified range (10-40 rad/s) of G''/ω vs G'/ω^2 for PG 46-34 at 100 Pa.

As the SLF model is derived from simple Hookean springs and Newtonian dashpots, it is entirely plausible that the highest frequency data would not conform to the trend. The Hookean model was originally developed for solid materials, specifically metals, that could only undergo small deformations. It is unsurprising that soft materials composed of larger molecules (like asphaltenes or polymer chains) capable of large deformations are no longer truly linear viscoelastic at high frequencies.

4.2.2 SLF parameters

Using Figure 4.7, the linear trendline can be fitted to eqn (2.17) to find the three material properties. First, the y-intercept represents μ_0, the viscosity of the stand-alone dashpot. Next, μ_1 is found from the difference of $(\mu_0 + \mu_1)$ generated from the $G''(\omega)$ data. Lastly, with μ_1 known, G can be calculated from the slope. Additionally, the ratio of μ_1/G (the inverse of the slope) gives τ_1, a "relaxation time" between the spring and dashpot in series. Table 4.1 contains the SLF parameters for all asphalt binders examined in this study.

Table 4.1 SLF parameters determined from 10-40 rad/s, 100 Pa data.

Material	$\mu_0 + \mu_1$ (Pa-s)	μ_0 (Pa-s)	μ_1 (Pa-s)	G (Pa)	τ_1 (s)
UNMODIFIED ASPHALTS					
PG 46-34	38.1	27.8	10.3	243.6	0.042
PG 58-28	173.6	153.0	20.6	379.8	0.054
PG 64-22	314.3	268.2	46.1	712.5	0.065
POLYMER MODIFIED ASPHALTS					
PG 58-37P	166.6	116.2	50.4	491.2	0.103
PG 64-34P	211.1	152.8	58.3	590.7	0.099
PG 70-31P	394.4	276.7	117.7	1048.3	0.112

The values of all material properties (μ_0, μ_1 and G) increased with an increase in the high-end PG designation, regardless of whether the binder was modified or not. For both, the increase in total viscosity was largely due to an increase in μ_0. Modified binders have greater μ_1 and G values. Between the binder sets, a notable difference in τ_1 is seen.

Unmodified binders have an increasing relaxation time τ_1 with grade. Modified binders, on the other hand, have comparable relaxation times amongst themselves that are approximately double the value of the unmodified binders. An increase in τ_1 indicates the addition of polymer has resulted in longer times to dissipate stress. It is interesting to note that colder PG grades may not need longer relaxation times (see PG 46-34 vs PG 64-22 and PG 58-37P vs PG 70-31P).

There are two sets of grades that have matching high-end, but different low-end temperatures. Comparing the PG 58-XX, although they have similar total viscosities, the polymer modified version has much more attributed to μ_1 (30% vs 12%). Despite also having a larger G value, this results in the polymer modified binder having a τ_1 that is 1.9× larger. Looking at the PG 64-XX, the polymer modified binder now has lower total viscosity and G value. However, a higher percentage of μ_1 (28% vs 15%) results in a τ_1 that is 1.5× larger for the polymer modified material. These results highlight the importance of μ_1 over other parameters, and thus, longer relaxation times in polymer modified binders.

As mentioned in Chapter 3, PG 70-31P is made by adding polymer to PG 58-28. Comparing these two binders, polymer addition has clearly increased all parameters, but not by the same amounts: Total viscosity increased by 2.3×, μ_0 by 1.8×, G by 2.8× and μ_1 by an astounding 5.7×. This results in a 2.1× larger τ_1 for the PG 70-31P. An increase in relaxation time is indicative of a slower rate of dissipation, but it also suggests that there is inherently more stress to dissipate. Between the two, it is natural to expect the polymer modified binder to recover more strain in a MSCR (multiple stress creep recovery) test.

4.3 MSCR Pulse Results

As discussed in §2.1.5, the SLF model is the simplest rheological model to qualitatively predict the response of asphalt binders under creep loading, specifically the MSCR test. Figure 4.8 displays the experimental and predicted strain responses to a MSCR pulse input for PG 70-31P. The MSCR pulse input was executed as detailed in §3.3.3. In this plot, the strain is scaled to the maximum amount occurring at 1 second (when the material begins recovering). By scaling the strain, the response of the SLF model is reduced to a single data

set independent of stress (due to the linear nature of the model). Furthermore, the time is intentionally only shown for the first 10 seconds to provide a better view of the response immediately after the creep portion ends. Although the majority of the strain recovery occurs in this window, a small amount is not shown in the time after the 10 second mark. Hence, the recovery amount shown here is not equal to the reported overall recovery discussed later.
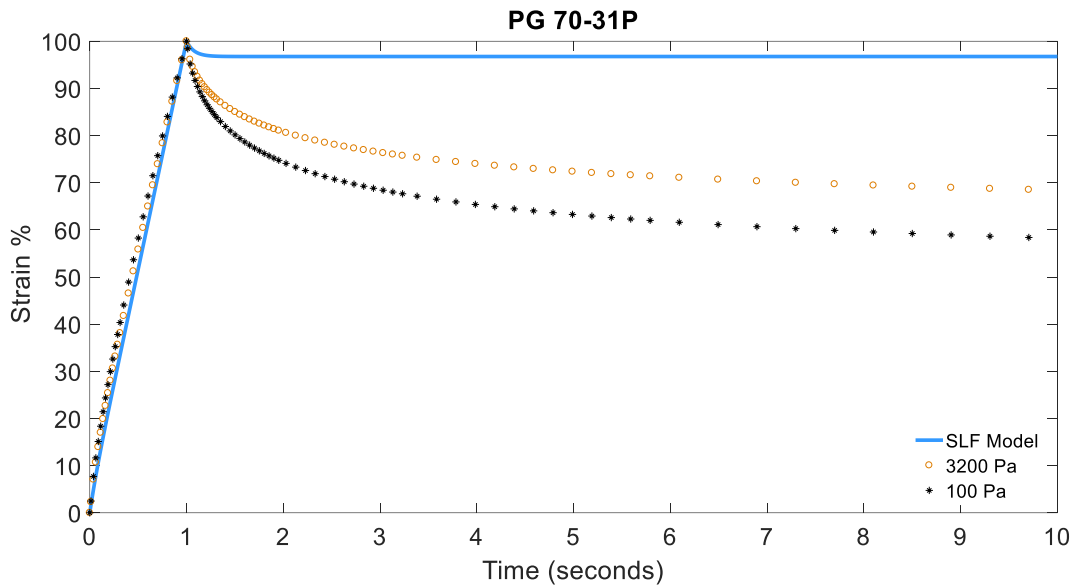
Figure 4.8 Predicted and Experimental MSCR Pulses for PG 70-31P.

During the creep portion, there is little difference between the high and low stresses, and the model predicts the increase in strain well. There is no instantaneous deformation, and a slight decrease in the rate of deformation as the creep is applied. Upon removal of the load, the binder only partially recovers as expected. However, during the recovery portion, the model is substantially under predicting the strain recovery amount. Even though the binder continues to recover with additional time, it is clear that the model prediction has no further recovery by the 2 second mark.

Comparing the binder responses, the recovery amount at 10 seconds decreases from approximately 40% to 30% as the stress is increased (remember that this is not the final recovery amount). This suggests that the recovery process is non-linear, which could explain why the SLF model underestimates the recovery amount. A closer look at the MSCR pulse

46

response for all materials is needed to determine if this non-linearity is due to the addition of polymer.

Table 4.2 summarizes the MSCR Pulse recovery data for all binders at both stresses, as well as two material parameters: τ_1 & $\%\mu_1$ (percentage μ_1 of the total viscosity). As was the case with the PG 70-31P, the recovery amount of all grades varied with stress, with the larger recoveries occurring at lower stresses. This might suggest that unmodified asphalts also have non-linear recovery. However, it is worth mentioning that the unmodified asphalts all finished recovering quickly, similar to what the SLF model predicts. In this sense, the recovery process is non-linear for asphalts, but the addition of polymer increases the deviation. Overall, the model predicts the unmodified asphalt recovery better than the polymer-modified counterparts. This is largely due to the fact that unmodified binders have such small recovery amounts (in some cases, the model overpredicts). This further reinforces the assertion that polymer modification increases non-linearity, as one would expect from macromolecules.

Table 4.2 Experimental and SLF predicted MSCR Pulse recovery data.

Material	τ_1 (s)	$\%\mu_1$ (%)	Experimental Recovery (%) 100 Pa	Experimental Recovery (%) 3200 Pa	SLF Predicted Recovery (%)
UNMODIFIED ASPHALTS					
PG 46-34	0.042	27.0	1.3	0.15	1.13
PG 58-28	0.054	11.9	1.5	0.30	0.64
PG 64-22	0.065	14.7	7.9	1.23	0.94
POLYMER MODIFIED ASPHALTS					
PG 58-37P	0.103	30.3	50.8	29.4	3.01
PG 64-34P	0.099	27.6	31.3	12.6	2.65
PG 70-31P	0.112	29.8	49.5	38.8	3.24

In §4.2.2, it was hypothesized that larger relaxation time τ_1 would indicate larger recovery amounts. Looking at the unmodified asphalt results, this is not necessarily the case. The predicted recovery for PG 46-34 is larger than for the other two grades, despite a smaller τ_1. Comparing all of their SLF parameters, we conclude that the $\%\mu_1$ is also an important factor

to consider when predicting recovery. Specifically, τ_1 is only useful when predicting expected recovery for materials with comparable $\%\mu_1$.

An examination of the $\%\mu_1$ of all materials reveals that PG 46-34 has a comparable ratio with the polymer modified binders. Interestingly, both the predicted recovery and τ_1 values for PG 46-34 are approximately 40% of the polymer modified grades. Together, these materials follow the general trend of larger τ_1 leading to more recovery. This trend is also followed in the remaining two binders — PG 58-28 and PG 64-22. As a check, keeping the $\%\mu_1$ constant, one can adjust the parameters in the SLF model to have larger τ_1 and will indeed find a larger predicted recovery.

It is worth determining what needs to be adjusted in the model to have reasonably accurate predictions of the polymer modified recovery amounts. Obviously, an increase in τ_1 is needed. There are two ways to accomplish this: increase μ_1, or decrease G. Using Matlab, a reduction of G from 1048.3 Pa to 300 Pa improves the predicted recovery amount to 10% for PG 70-31P. However, this is still not enough to match the experimental results despite an increase in τ_1 by 3.5×. Further increasing τ_1 to 8.75×, via increasing the viscosity ratio by 2.5× results in a recovery of approximately 40% (our desired amount). Figure 4.9 adds this "curve-fit" version of the SLF model to the previously discussed MSCR pulse results.
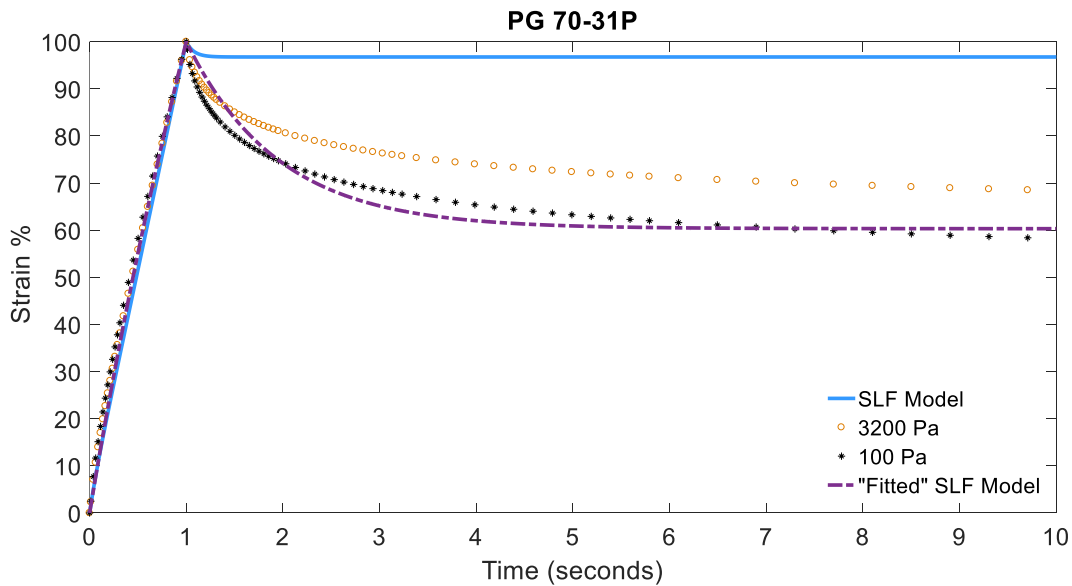

Figure 4.9 Fitted SLF MSCR Pulse prediction for PG 70-31P.

Clearly, significant changes must be made to the parameters to accurately predict the recovery amount. Although this theoretical value of G is comparable to those determined from the binders used in this study, the required theoretical viscosity values are much larger than all cases. Furthermore, the procedure to acquire the SLF parameters cannot be adjusted to produce smaller values of G and such large viscosity values. A comparison between the frequency sweep and the MSCR pulse excitations reveals a possible reason for the discrepancy in the SLF predictions of the experimental results.

4.4 Sources of Non-Linearity

Thus far, we have seen that the SLF model is capable of predicting the shape of the MSCR pulse correctly, but it does not accurately quantify the response. When comparing the experimental results, it is apparent that the recovery portion is non-linear, as the amount of strain that is recovered varies with the stress applied. This is the opposite conclusion to what was reached at the beginning of this chapter, when we saw that the oscillatory frequency sweep response did not change with stress level.

Oscillatory excitations require small amounts of deformation to preserve the integrity of the sample. If too large of a deformation is used, some portion of the sample will inevitably flow out of the space between the plates. During the acquisition of the frequency sweep data, the amount of deformation used is determined by the software automatically. Creep excitations on the other hand, do not have any constraint imposed on the amount of strain. The amount of deformation depends entirely on the inputs used *and* time allowed.

Table 4.3 compares the strain experienced by the binders at 100 Pa for both the frequency sweep and MSCR pulse excitations. Here, 100% strain is equivalent to 1 revolution of the top plate. For the oscillatory data, the strain amount decreased as the angular frequency increases. This makes sense intuitively, as higher frequencies subject the binder to larger shear stress, and thus, a smaller amount of strain is required to preserve the sample. All but one strain amount is below 5.7% in the oscillatory data. This is considerably less than the minimum amount of 13.5% in the MSCR pulse data (keep in mind, the 3200 Pa data are approximately 32× the values shown here)

Table 4.3 Frequency sweep and MSCR pulse excitations strain percentages for 100 Pa.

	Oscillation Strain %		MSCR Strain %
Material	10 rad/s	80 rad/s	(maximum)
UNMODIFIED ASPHALTS			
PG 46-34	25.2	1.3	119
PG 58-28	5.7	0.8	52.3
PG 64-22	3.1	0.5	14.6
POLYMER MODIFIED ASPHALTS			
PG 58-37P	5.4	1.1	18.9
PG 64-34P	4.3	0.8	29.2
PG 70-31P	2.2	0.5	13.5

As mentioned previously, the Hookean model was originally developed for solid materials that could only undergo small deformations, similar to the oscillatory frequency sweeps. As oscillatory data was used to determine the SLF parameters, it is reasonable to expect that those parameters are no longer valid for excitations with large deformations like the MSCR pulse. These results further reinforce the notion that asphalt binders (whether unmodified or polymer modified) are not linear viscoelastic materials during the recovery portion of the MSCR. Ultimately, the recovery process is non-linear in nature and therefore unrealistic to expect the Standard Linear Fluid model to accurately predict the MSCR response.

4.5 Non-Linear Modelling

It was ambitious to use a rheological model composed of only linear relations to predict excitations that produce large deformations. An alternative to the SLF model utilized so far is the inclusion of non-linear elements. In general, a model can be considered non-linear if any of the elements describe their stress-strain relationship non-linearly. In our scenario, we are mostly concerned with the underpredicting of the recovery amount for a MSCR pulse excitation. Thus, our focus is on the elastic element in our model. We hypothesize that instead of a linear relation (like a Hookean spring), a "hyperelastic" relationship is more appropriate. Hyperelastic models are used to describe stress-strain relationships of elastic materials that are non-linear. Rubber is a well-known hyperelastic material, and has

similarities to the soft, large macromolecules of polymer modified asphalt binders [32]. One possible hyperelastic constitutive model is the Mooney-Rivlin (M-R) model. It considered to be suitable for deformations up to 100% [33]. By replacing the elastic spring in the SLF model with hyperelastic element akin to the M-R model, we have the modified SLF model. (This modified version of the SLF model is of course, non-linear, despite the namesake).
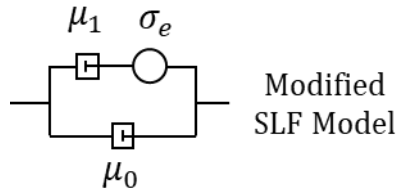
Figure 4.10 Schematic of the proposed modified SLF model.

This model introduces two material constants as additional parameters, a and b. These are used in combination with G (the elastic modulus determined from the frequency sweep data) to model the elastic stress function by the following equations:

$$\sigma_e = a\left[1 - \exp\left(-\frac{b\varepsilon_e}{a}\right)\right] + (G - b)\varepsilon_e \tag{4.1}$$

$$\frac{d\sigma_e}{d\varepsilon_e} = b\exp\left(-\frac{b\varepsilon_e}{a}\right) + (G - b) \tag{4.2}$$

and depicted by this sketch of the elastic stress-strain curve.
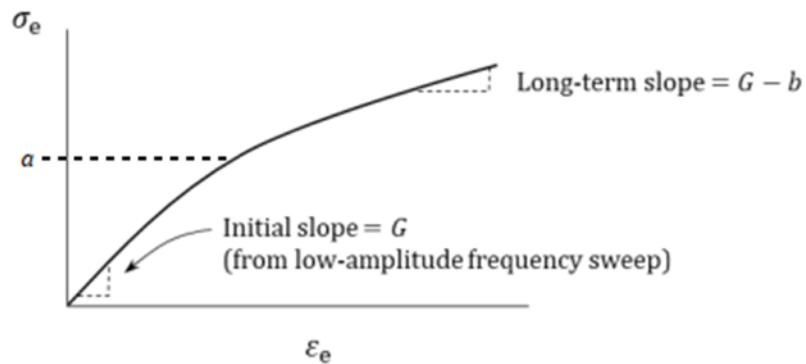
With the aid of Matlab, a MSCR excitation response was generated using the modified SLF model with $a = 350$ Pa and $b = 1000$ Pa (it is worth noting these values were chosen purely in the interest of improving the prediction) and the SLF model parameters for PG 70-31P as shown in Figure 4.11. The modified model predicts the recovery amount better than the original SLF model while maintaining the required response shape. There is no instantaneous deformation or recovery upon onset or removal of the load. However, the amount of time needed to fully recover is still too fast, and there is an abrupt end to the recovery instead of a more gradual gain over time like the experimental results. Still, despite these inaccuracies, a predicted recovery amount of nearly 20% is a remarkable improvement compared to the 3% predicted by the original SLF model.
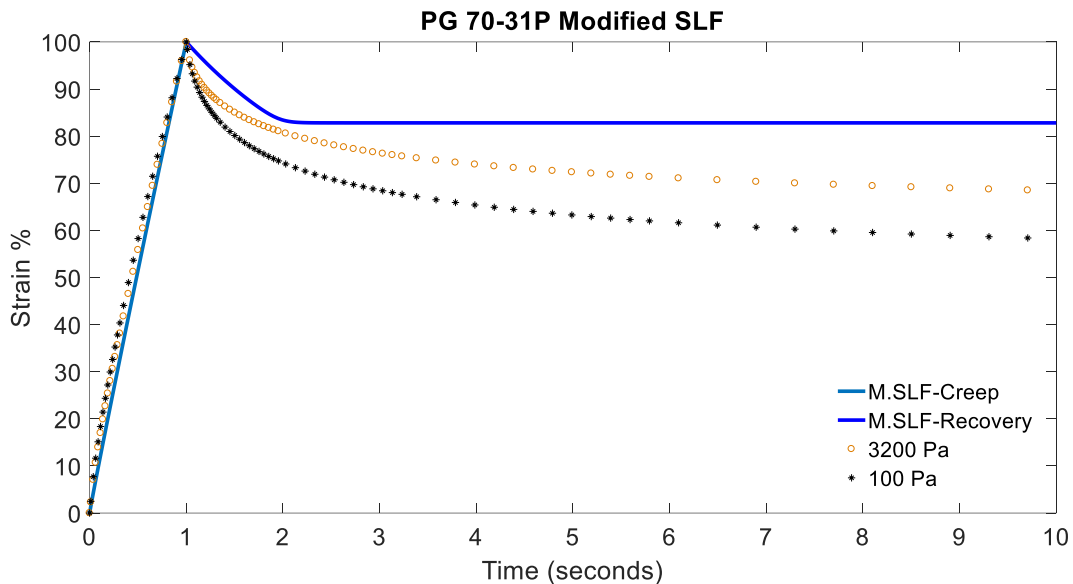
Figure 4.11 Modified SLF MSCR Pulse prediction for PG 70-31P.

The results of the modified SLF model confirm that the best approach to predict the MSCR response (with large deformation) requires inclusion of non-linear elements. The reduction of slope in the long term allows an increased amount of elastic (and thus recoverable) strain. It is possible that reconsidering one or both viscosity elements to also be non-linear in nature would improve the MSCR prediction even further. However, this idea is left for future work.

Chapter 5: Conclusions and Future Work

We have introduced a simple, lowest-order rheological model — the Standard Linear Fluid (SLF) model — that is capable of predicting the MSCR response. It was shown that by performing a Frequency Sweep with a Dynamic Shear Rheometer, the SLF model parameters of asphalt binders can be determined. Furthermore, these parameters can be used to distinguish between polymer-modified and unmodified asphalts, just as a MSCR test can.

However, the original goal of this thesis was to predict the MSCR response. Although the model can predict the creep portion of the test, it failed to accurately predict the amount of strain that was recovered. Variation in the amount of experimental recovery suggested that this recovery portion must be non-linear in nature, whether or not the asphalt has been modified with polymer. As the SLF model inherently assumes linearity for stress-strain relationships, it cannot predict this non-linear relaxation of stress.

It was determined that the root cause of the non-linearity was likely due to the large amount of deformation experienced in MSCR testing. It was therefore unrealistic to expect the linear SLF model (whose parameters are determined from small deformation excitations) to accurately predict the response of large deformations seen in the MSCR test. An adjustment was made to the elastic element of the SLF model to account for non-linearity due to large deformation in the form of a Mooney-Rivlin model. This improved the prediction for the recovery portion of the MSCR test considerably, but still not enough to agree with the experimental results at the cost of two additional parameters. Insight was gained on the impact of representing the amount of elastic strain in a non-linear fashion to the predicted MSCR recovery amount.

This thesis has made significant contributions towards the rheological modeling of asphalt materials. The SLF model only has three parameters, while still capturing the underlying physics of the material. Other models discussed in asphalt rheology either assume an infinite number of rheological elements or cannot correctly predict the shape of the MSCR response.

Lastly, we have also presented a straightforward protocol to determine the SLF parameters. Despite this research only being concerned with asphalt rheology, there is potential for other

industries to further their rheological understanding. Materials similar in nature to the ones we have discussed here, namely, large molecules with potential for elastic characteristics, could also make use of the SLF model. Although we have shown that the SLF model cannot quantitatively predict our MSCR excitation, that does not mean all excitations cannot be predicted.

Some considerations for future work include the following:

- Investigate how large of a range of deformation for the oscillatory input can be used to determine the SLF parameters. This can involve changing strain/stress levels used but also other parameters such as the gap height.

- Comparing the SLF prediction when the stress level is reduced in the MSCR pulse excitation to a comparable amount of deformation used in the frequency sweep excitation to determine the SLF parameters.

- Analyze the quality of the data for the frequency sweep using angular frequencies below 10 rad/s. Ideally, getting a close to the zero-frequency limit as possible.

- Assess the SLF model's prediction ability when one or both viscosity elements is replaced with non-linear relationships.

References

[1]   Transport Canada, "Transportation in Canada 2018," 2018. [Online]. Available: https://tc.canada.ca/sites/default/files/migrated/transportation_in_canada_2018. pdf. [Accessed February 2020].

[2]   US Department of Transportation Federal Highway Administration, 27 November 2018. [Online]. Available: https://www.fhwa.dot.gov/policyinformation/statistics/ 2017/hm20.cfm. [Accessed February 2020].

[3]   Asphalt Insitute, "How Many U.S. Roads Are Paved With Asphalt?," 2015. [Online]. Available: http://asphaltmagazine.com/how-many-u-s-roads-are-paved-with- asphalt/. [Accessed February 2020].

[4]   P. S. Kandhal, "History of ASTM Committee D04 on Road and Paving Materials, 1903- 2003," September 2003. [Online]. [Accessed February 2020].

[5]   ASTM D5/ D5M-20, "Standard Test Method for Penetration of Bituminous Materials," 2020. [Online]. Available: http://www.astm.org/cgi-bin/resolver.cgi?D5D5M.

[6]   ASTM D2170 / D2170M-18, "Standard Test Method for Kinematic Viscosity of Asphalts", ASTM International, West Conshohocken, PA," 2018. [Online]. Available: http://www.astm.org/cgi-bin/resolver.cgi?D2170D2170M.

[7]   ASTM D2171 / D2171M-18, "Standard Test Method for Viscosity of Asphalts by Vacuum Capillary Viscometer", ASTM International, West Conshohocken, PA," 2018. [Online]. Available: http://www.astm.org/cgi-bin/resolver.cgi?D2171D2171M.

[8]   ASTM D7175-15, "Standard Test Method for Determining the Rheological Properties of Asphalt Binder Using a Dynamic Shear Rheometer", ASTM International, West Conshohocken, PA," 2015. [Online]. Available: http://www.astm.org/cgi- bin/resolver.cgi?D7175.

[9]   ASTM D6816-11(2016), "Standard Practice for Determining Low-Temperature Performance Grade (PG) of Asphalt Binders", ASTM International, West Conshohocken, PA," 2016. [Online].

[10]   AASHTO M320,"Standard Specification for PerformanceGraded Asphalt Binder," 2017

[11] "Permanent Deformation Rutting Classification," Roadex Network, [Online]. Available: https://www.roadex.org/e-learning/lessons/permanent-deformation/permanent-deformation-rutting-classification/. [Accessed Jan 2020].

[12] Y. Tang and J. E. Haddock, "Investigation of The Performance Of Neat And Modified Asphalt Binders," Purdue University, West Lafayette, IN, 2006.

[13] Pavement Interactive, "Superpave Performance Grading," [Online]. Available: https://pavementinteractive.org/reference-desk/materials/asphalt/superpave-performance-grading/. [Accessed January 2020].

[14] G. Baumgardner, "Multiple Stress Creep and Recovery (MSCR) Implementation and Transition," University of Nevada, Reno, Nevada, 2020.

[15] Edward Harrigan, "High Temperature Performance I-80 Nevada," National Cooperative Highway Research Program, 2003.

[16] M. J. Khattak and G. Y. Baladi, "Engineering Properties of Polymer Modifed Asphalt Mixtures," *Transportation Research Board,* no. 1638, pp. 12-22, 1998.

[17] Y. Becker, M. P. Méndez and Y. Rodríg, "Polymer Modified Asphalt," *Vision Tecnologica,* vol. 9, pp. 39-50, 2001.

[18] M. Anderson, "Introduction to the Multiple-Stress Creep-Recovery (MSCR) Test," in *54th Annual Idaho Asphalt Conference*, Moscow, Idaho, 2014.

[19] ASTM D7405-20, "Standard Test Method for Multiple Stress Creep and Recovery (MSCR) of Asphalt Binder Using a Dynamic Shear Rheometer", ASTM International, West Conshohocken, PA," 2020. [Online]. Available: http://www.astm.org/cgi-bin/resolver.cgi?D7405. [Accessed January 2020].

[20] US Department of Transportation Federal Highway Administration, "The Multiple Stress Creep Recovery (MSCR) Procedure," 2011.

[21] D. Singh and D. Sawant, "Understanding Effects of RAP on Rheological Performance and Chemical Composition of SBS Modified Binder Using Series of Laboratory Tests," *International Journal of Pavement Research and Technology,* vol. 9, pp. 178-189, 2016.

[22] W. Flugge, Viscoelasticity 2nd edn., New York: Springer Verlag, 1975.

[23] W. N. Findley, J. Lai and K. Onaran, Creep and Relaxtion of Nonlinear Viscoelastic Materials, Amsterdam: North-Holland Publishing, 1976.

[24] A. Y. Malkin and A. I. Isayev, Rheology: Concepts, Methods and Applications 2nd edn., Toronto: ChemTec Publishing, 2012.

[25] M. L. Williams, R. F. Landel and J. D. Ferry, "The Temperature Dependence of Relaxation Mechanisms in Amorphous Polymers and Other Glass-forming Liquids," *Journal of American Chemical Society,* vol. 77, no. 14, pp. 3701-3707, 1955.

[26] F. Olard and H. Benedetto, "General "2S2P1DModel and Relation Between the Linear Viscoelastic Behaviours of Bituminous Binders and Mixes," *Road Materials and Pavement Design,* vol. 4, no. 2, pp. 185-224, 2003.

[27] A. Blasl, M. Khalili, G. Falla, M. Oeser and P. W. F. Liu, "Rheological characterisation and modelling of bitumen containing reclaimed components.," *Int. J. Pavement Eng,* vol. 20, no. 6, pp. 638-648, 2019.

[28] Q. Xu and M. Solaimanian, "Modelling linear viscoelastic properties of asphalt concret by the Huet–Sayegh model," *Int. J. Pavement Eng,* vol. 10, no. 6, pp. 401-422, 2009.

[29] D. W. J. Christensen, "Mathematical modeling of the linear viscoelastic behavior of asphalt cements (Doctoral Disseration)," The Pennsylvania State University, 1992.

[30] D. W. Christensen, D. A. Anderson and G. M. Rowe, "Relaxation spectra of asphalt binders and the," *Road Materials and Pavement Design,* vol. 18, pp. 382-403, 2017.

[31] TA Instruments, "DHR Getting Started Guide," April 2013. [Online]. Available: https://pages.mtu.edu/~fmorriso/cm4655/TAInstruments/2013TA_DHRGettingSta rtedGuide.pdf. [Accessed June 2019].

[32] H. Khajehsaeid, J. Arghavani and R. Naghdabadi, "A hyperelastic constitutive model for rubber-like materials," *European Journal of Mechanics - A/Solids,* vol. 38, no. March-April, pp. 144-151, 2013.

[33] M. N. Hamza and H. M. Alwan, "Hyperelastic Constitutive Modeling of Rubber and Rubber- Like Materials under Finite Strain," *Engineering and Technology Journal,* vol. 28, no. 13, pp. 2560-2575, 2010.

Appendix A1: Frequency Sweep Data

PG 46-34											
	1 Pa			10 Pa			100 Pa				
Angular frequency	Storage modulus	Loss modulus	tan (delta)	Storage modulus	Loss modulus	tan (delta)	Storage modulus	Loss modulus	tan (delta)		
rad/s	Pa	Pa		Pa	Pa		Pa	Pa			
10	50.83	389.88	7.67	44.20	382.81	8.66	44.53	382.62	8.59		
15	102.57	577.42	5.63	95.50	569.62	5.96	96.36	569.88	5.91		
20	172.84	765.69	4.43	164.59	754.26	4.58	166.27	754.55	4.54		
25	259.88	948.30	3.65	251.77	934.72	3.71	253.68	937.44	3.70		
30	370.11	1121.04	3.03	356.86	1114.91	3.12	358.97	1117.79	3.11		
35	490.54	1306.82	2.66	478.90	1297.14	2.71	481.08	1298.15	2.70		
40	633.47	1487.49	2.35	618.66	1473.68	2.38	620.38	1475.77	2.38		
60	1360.84	2191.92	1.61	1346.30	2171.48	1.61	1354.65	2176.31	1.61		
80	2390.14	2924.71	1.22	2338.63	2855.45	1.22	2345.08	2864.57	1.22		

PG 58-28											
	1 Pa			10 Pa			100 Pa				
Angular frequency	Storage modulus	Loss modulus	tan (delta)	Storage modulus	Loss modulus	tan (delta)	Storage modulus	Loss modulus	tan (delta)		
rad/s	Pa	Pa		Pa	Pa		Pa	Pa			
10	130.64	1691.42	12.95	132.57	1718.88	12.97	131.53	1760.84	13.39		
15	223.91	2479.61	11.07	227.07	2517.97	11.09	228.28	2587.95	11.34		
20	325.64	3253.34	9.99	331.19	3303.81	9.98	333.34	3393.15	10.18		
25	434.66	4013.01	9.23	441.53	4069.08	9.22	444.66	4167.75	9.37		
30	551.59	4747.39	8.61	557.22	4831.04	8.67	562.80	4937.31	8.77		
35	669.37	5502.18	8.22	676.53	5570.72	8.23	685.42	5700.51	8.32		
40	784.17	6226.33	7.94	797.86	6312.73	7.91	810.84	6448.62	7.95		
60	1317.78	9028.75	6.85	1325.65	9139.83	6.89	1347.47	9339.24	6.93		
80	1912.63	11699.62	6.12	1891.72	11891.88	6.29	1937.68	12090.27	6.24		

PG 64-22											
	1 Pa			10 Pa			100 Pa				
Angular frequency	Storage modulus	Loss modulus	tan (delta)	Storage modulus	Loss modulus	tan (delta)	Storage modulus	Loss modulus	tan (delta)		
rad/s	Pa	Pa		Pa	Pa		Pa	Pa			
10	356.87	3264.68	9.15	356.67	3206.71	8.99	359.45	3222.00	8.96		
15	606.13	4661.29	7.69	607.36	4662.05	7.68	611.26	4662.39	7.63		
20	881.19	6068.91	6.89	886.01	6069.55	6.85	894.01	6117.21	6.84		
25	1188.32	7542.07	6.35	1191.18	7455.86	6.26	1195.69	7448.93	6.23		
30	1524.58	8871.68	5.82	1518.35	8843.11	5.82	1523.64	8863.47	5.82		
35	1853.40	10179.30	5.49	1860.69	10111.50	5.43	1868.87	10148.20	5.43		
40	2201.33	11500.40	5.22	2220.37	11463.10	5.16	2233.48	11536.30	5.17		
60	3838.09	16460.00	4.29	3848.28	16444.60	4.27	3872.93	16485.70	4.26		
80	5754.57	21591.20	3.75	5763.55	21345.00	3.70	5809.85	21146.80	3.64		

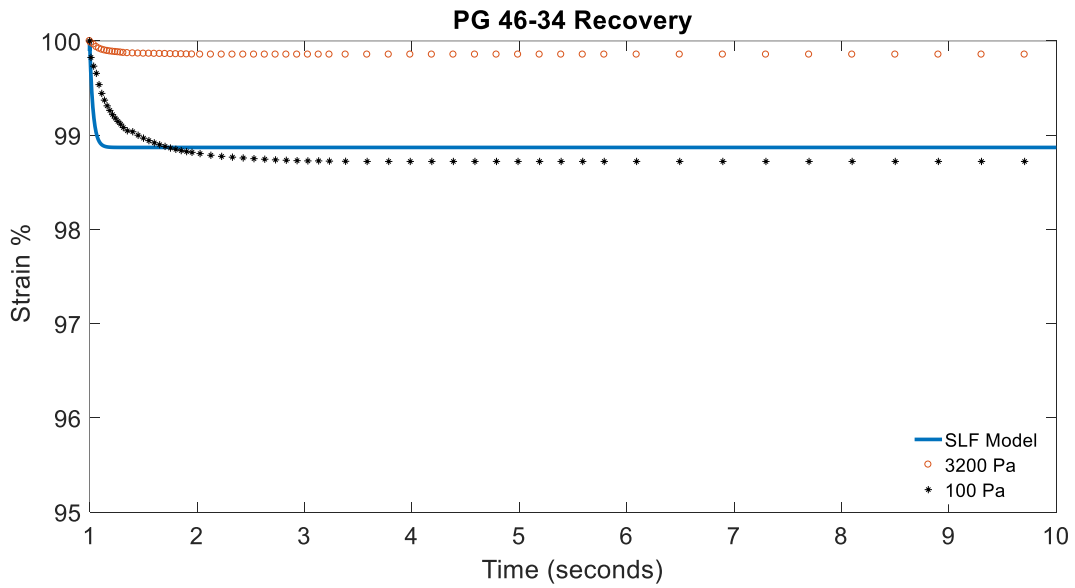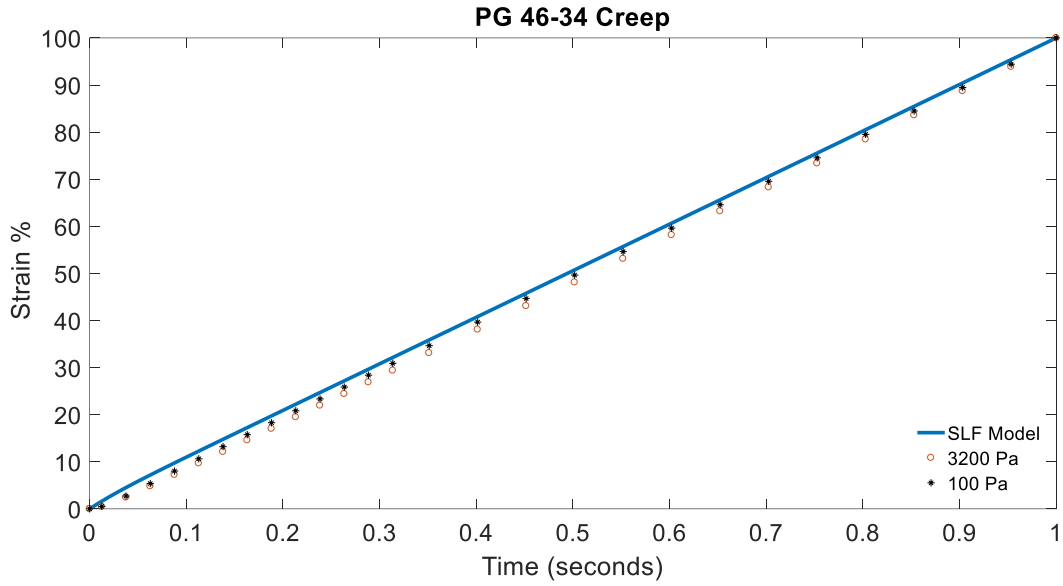| PG 58-37P									
	1 Pa			10 Pa			100 Pa		
Angular frequency rad/s	Storage modulus Pa	Loss modulus Pa	tan (delta)	Storage modulus Pa	Loss modulus Pa	tan (delta)	Storage modulus Pa	Loss modulus Pa	tan (delta)
10	679.26	1778.27	2.62	668.45	1782.90	2.67	667.24	1778.31	2.67
15	981.07	2432.21	2.48	969.77	2429.33	2.51	967.79	2425.08	2.51
20	1274.01	3024.17	2.37	1265.01	3025.59	2.39	1264.22	3016.75	2.39
25	1577.95	3594.09	2.28	1562.62	3577.71	2.29	1563.04	3570.27	2.28
30	1878.25	4119.13	2.19	1867.29	4111.57	2.20	1866.74	4095.56	2.19
35	2185.68	4600.50	2.10	2178.14	4628.91	2.13	2179.06	4608.17	2.11
40	2504.45	5091.24	2.03	2499.55	5108.50	2.04	2498.97	5085.44	2.04
60	3892.41	6938.39	1.78	3886.52	6921.41	1.78	3893.28	6913.00	1.78
80	5341.22	8694.03	1.63	5476.61	8602.66	1.57	5482.37	8585.42	1.57

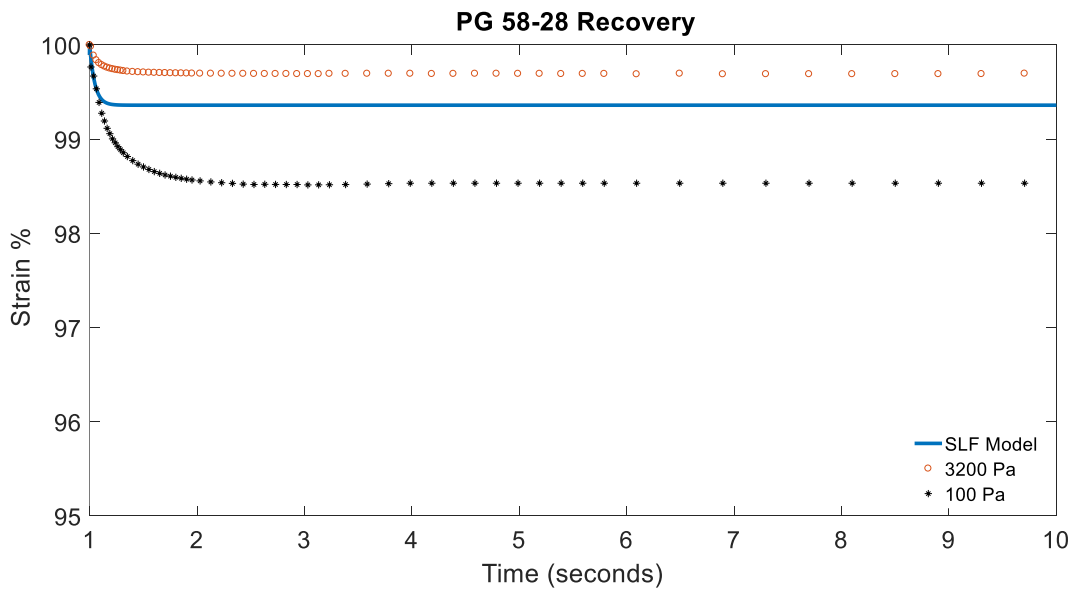| PG 64-34P									
	1 Pa			10 Pa			100 Pa		
Angular frequency rad/s	Storage modulus Pa	Loss modulus Pa	tan (delta)	Storage modulus Pa	Loss modulus Pa	tan (delta)	Storage modulus Pa	Loss modulus Pa	tan (delta)
10	757.16	2271.90	3.00	764.57	2266.88	2.96	755.70	2256.64	2.99
15	1112.40	3144.04	2.83	1116.93	3116.15	2.79	1097.89	3069.49	2.80
20	1444.92	3907.21	2.70	1462.09	3899.05	2.67	1465.85	3938.83	2.69
25	1778.11	4589.87	2.58	1812.12	4641.98	2.56	1791.21	4565.75	2.55
30	2144.99	5337.90	2.49	2171.23	5353.30	2.47	2146.81	5275.21	2.46
35	2518.43	6082.61	2.42	2533.58	6022.17	2.38	2531.46	6140.28	2.43
40	2857.73	6692.57	2.34	2899.68	6673.05	2.30	2873.85	6553.00	2.28
60	4457.51	9127.81	2.05	4482.59	9144.16	2.04	4467.43	8956.03	2.00
80	6358.60	11532.60	1.81	6253.66	11439.60	1.83	6221.30	11345.10	1.82

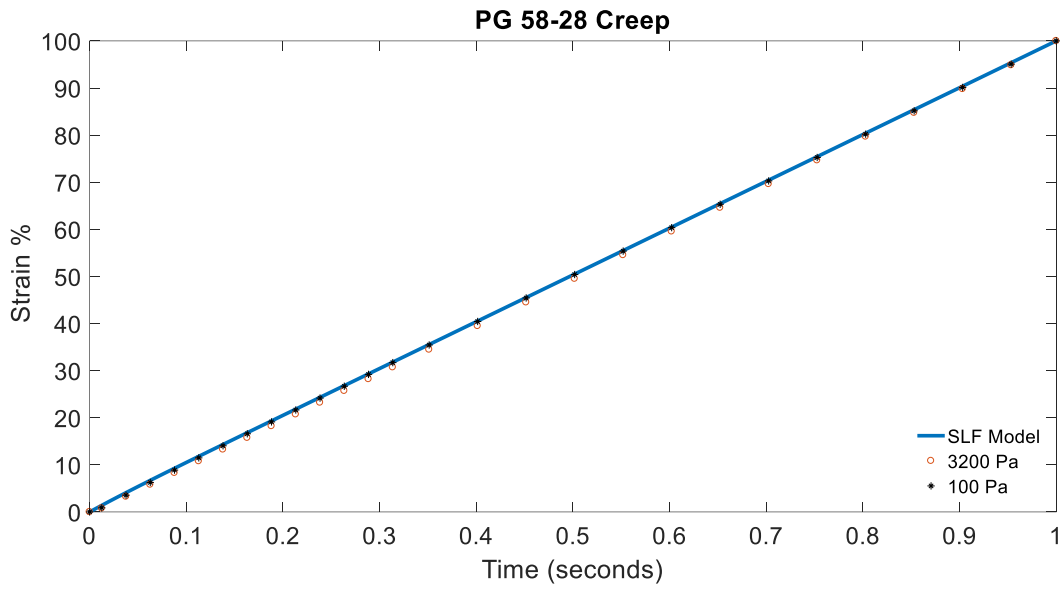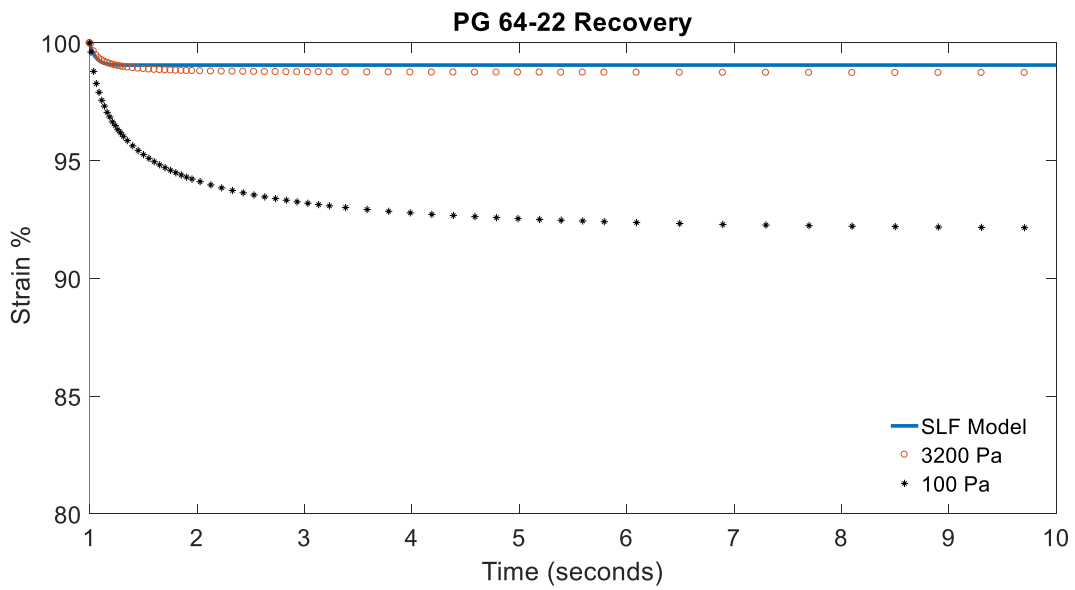| PG 70-31P									
	1 Pa			10 Pa			100 Pa		
Angular frequency rad/s	Storage modulus Pa	Loss modulus Pa	tan (delta)	Storage modulus Pa	Loss modulus Pa	tan (delta)	Storage modulus Pa	Loss modulus Pa	tan (delta)
10	1745.25	4214.35	2.41	1740.67	4220.42	2.42	1741.44	4229.51	2.43
15	2394.30	5659.42	2.36	2425.19	5719.10	2.36	2422.39	5724.78	2.36
20	3102.31	7140.69	2.30	3060.12	7085.21	2.32	3067.33	7102.72	2.32
25	3664.29	8327.84	2.27	3681.08	8373.90	2.27	3688.86	8389.33	2.27
30	4253.37	9509.05	2.24	4291.13	9596.90	2.24	4279.92	9570.52	2.24
35	4903.01	10763.10	2.20	4889.14	10762.90	2.20	4876.71	10727.70	2.20
40	5471.18	11863.60	2.17	5482.92	11885.70	2.17	5467.19	11831.40	2.16
60	7751.27	15965.00	2.06	7890.84	16092.40	2.04	7878.37	16043.20	2.04
80	10467.00	20350.30	1.94	10440.20	19976.90	1.91	10393.30	19913.40	1.92

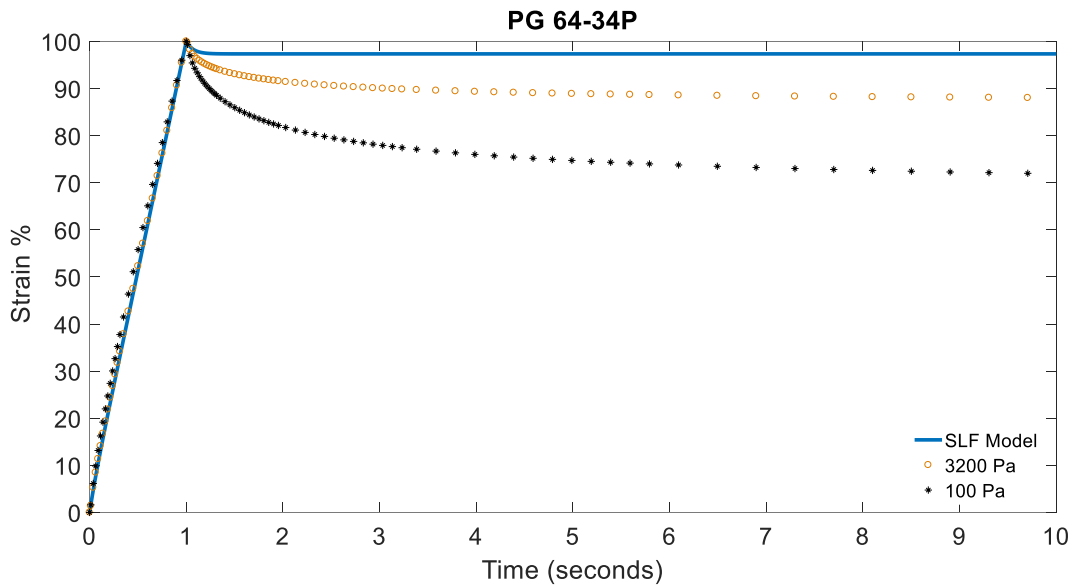# Appendix A2: Additional MSCR Pulse Figures

PG 46-34:

PG 58-28:

PG 58-28 Creep

PG 58-28 Recovery

PG 64-22:

PG 64-22 Creep
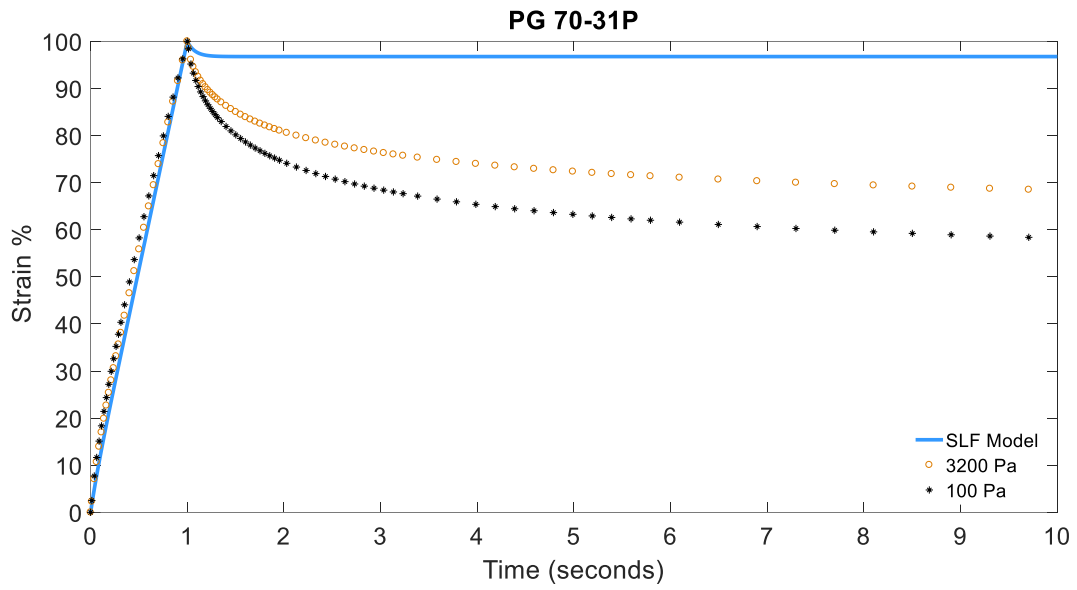

PG 64-22 Recovery
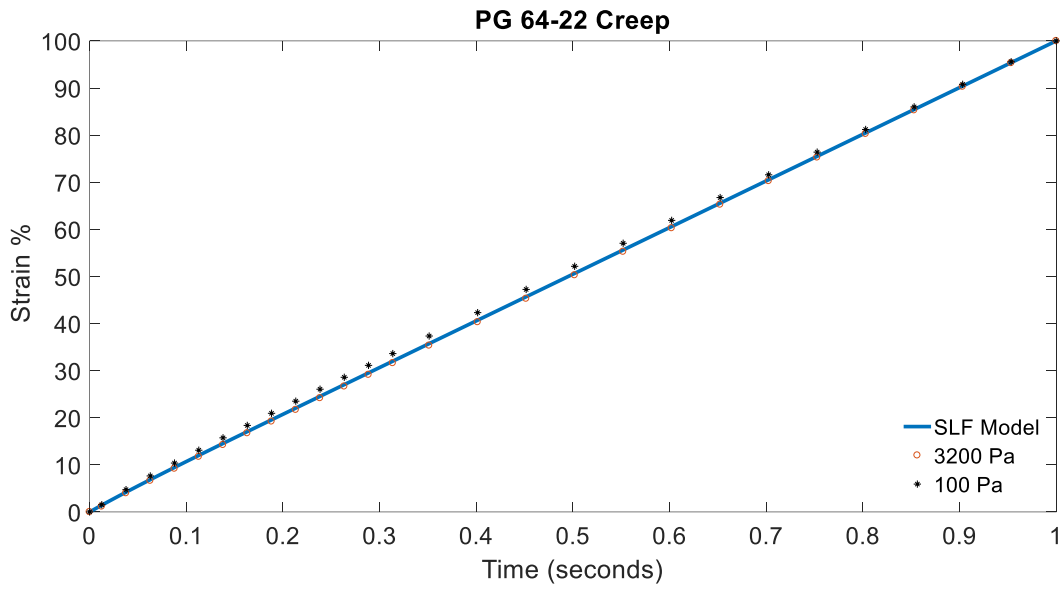
PG 58-37P:
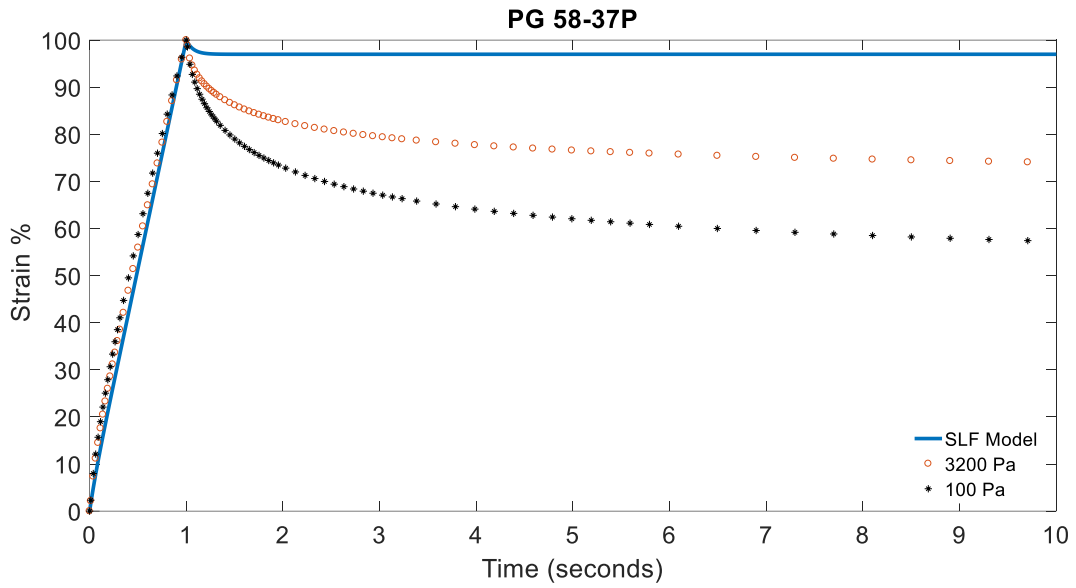
PG 64-34P:

PG 70-31P:

PG 70-31P

Appendix B1: SLF Parameter Sample Calculations

Here is an example of how to solve for the SLF Parameters using the 100 Pa Frequency Sweep data for PG 58-28:

PG 58-28	100 Pa		
Angular frequency rad/s	Storage modulus Pa	Loss modulus Pa	tan (delta)
10	131.53	1760.84	13.39
15	228.28	2587.95	11.34
20	333.34	3393.15	10.18
25	444.66	4167.75	9.37
30	562.8	4937.31	8.77
35	685.42	5700.51	8.32
40	810.84	6448.62	7.95
60	1347.47	9339.24	6.93
80	1937.68	12090.27	6.24

Plotting the loss modulus (G'') vs angular frequency (ω) gives:

G'' vs ω (PG 58-28)
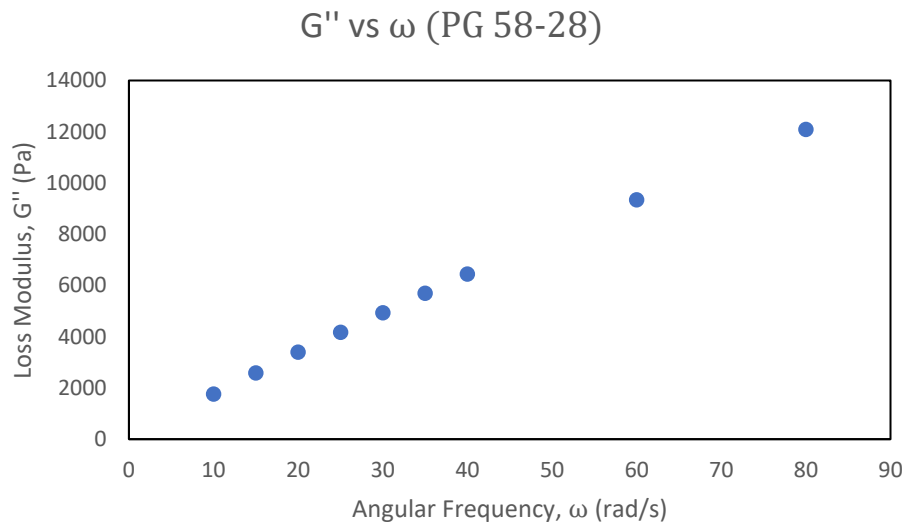
Next, a linear trendline that is forced through the origin is fit to the data. We decided to only use the first two data points as they are our lowest frequency, and we are trying to

find the "zero-frequency viscosity". A linear trendline for the whole data set is shown to see that the difference is small, but noticeable. Other data sets may have a larger difference.

G'' vs ω (PG 58-28)

y = 156.66x

y = 173.62x
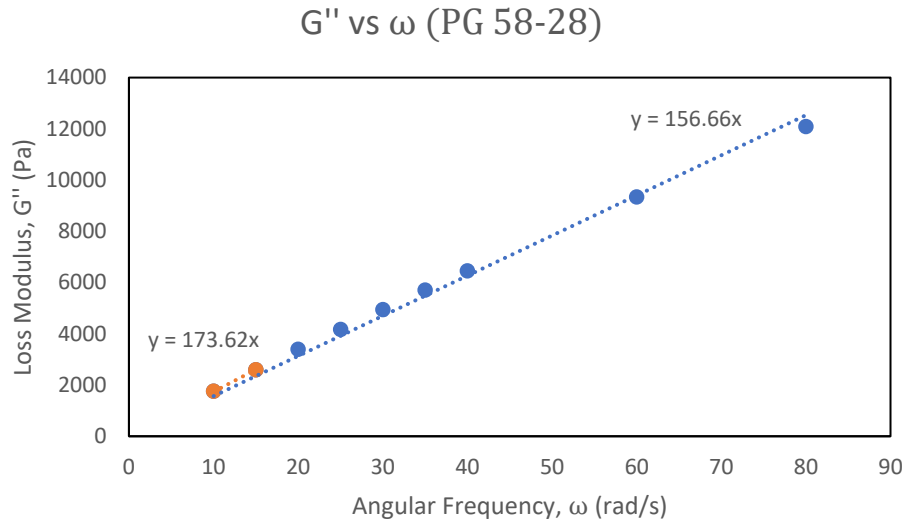
The slope of the trendline is set as the value of $\mu_0 + \mu_1$, therefore:
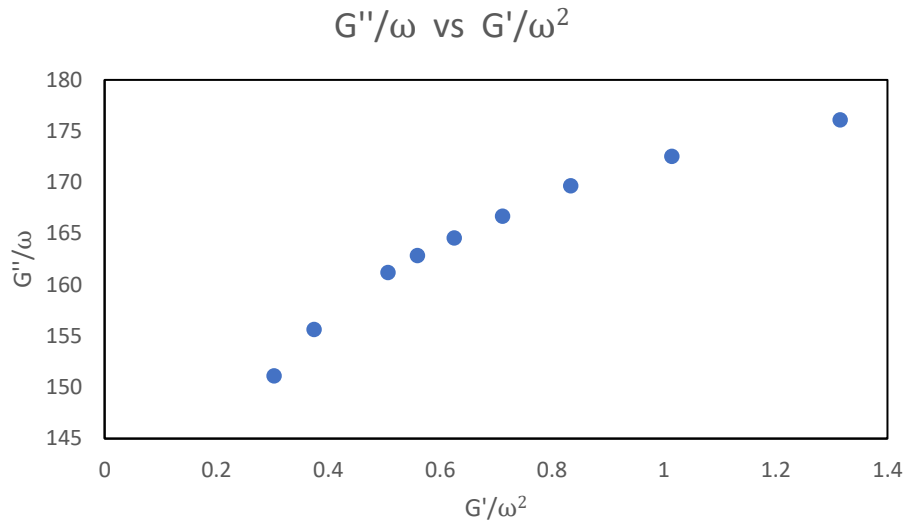
$$\mu_0 + \mu_1 = 173.62 \; Pa \cdot s$$

Recall that we are trying to fit our data to equation (2.17):

$$\frac{G''}{\omega} = \frac{G}{\mu_1} \frac{G'}{\omega^2} + \mu_0$$

Next, the values of G''/ω vs G'/ω^2 are calculated and plotted.

w	G''/w	G'/w²
10	176.08	1.32
15	172.53	1.01
20	169.66	0.83
25	166.71	0.71
30	164.58	0.63
35	162.87	0.56
40	161.22	0.51
60	155.65	0.37
80	151.13	0.30

G''/ω vs G'/ω²

Again, a linear trendline is fit to this dataset. We noticed that the highest frequency data points begin to deviate from the linear slope of the lower frequency points, so they were excluded. Trendlines for both the entire set and the reduced set are shown to see the improvement in the fit. Remember that we are working with a linear model, so a better linear fit is ideal.

G''/ω vs G'/ω²

y = 18.429x + 153.01
R² = 0.9681

y = 23.632x + 148.1
R² = 0.9165
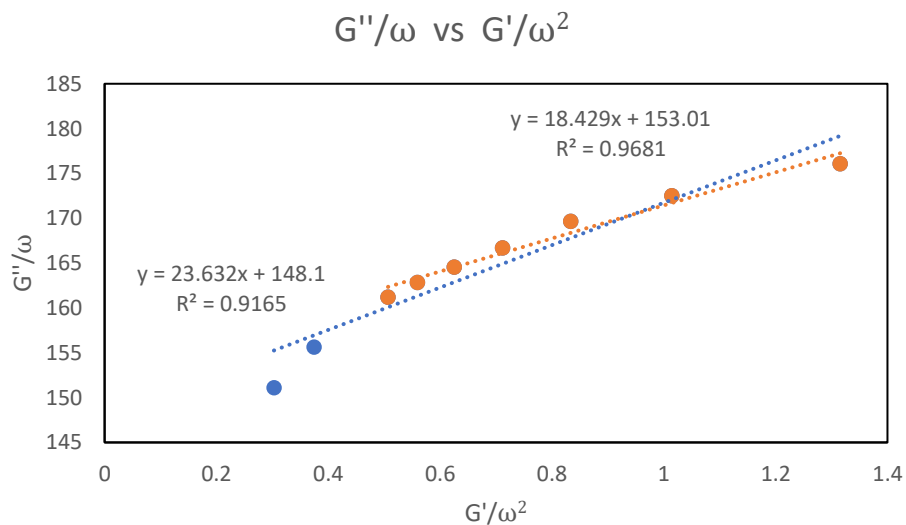
From this trendline we can gather that:

$$\mu_0 = 153.01 \; Pa \cdot s$$

$$G/\mu_1 = 18.429 \; s^{-1}$$

Our previous work found:

$$\mu_0 + \mu_1 = 173.62 \; Pa \cdot s$$

Therefore:

$$\mu_1 = 173.62 - \mu_0 = 173.62 - 153.01 = 20.61 \; Pa \cdot s$$

$$G = 18.429 * \mu_1 = 18.429 * 20.61 = 379.82 \; Pa$$

Lastly, we can calculate τ_1 as follows:

$$\tau_1 = \frac{\mu_1}{G} = \frac{20.61}{379.82} = 0.054s$$

Or alternatively,

$$\tau_1 = \frac{1}{18.429} = 0.054s$$

To summarize, we have found the SLF parameters for PG 58-28 to be:

$$\mu_0 = 153.01 \; Pa \cdot s$$

$$\mu_1 = 20.61 \; Pa \cdot s$$

$$G = 379.82 \; Pa$$

Appendix B2: Sample Matlab Code for SLF MSCR Prediction

```matlab
%% MSCR Pulse Input
%Evan Kohut March 2020
clc; clear all; close all;
%Analytical solution from chapter 2 draft
---------------------------------------------------

%% Inputs
%SLF parameters (Example for PG 70-31P)
mu_knot = 276.7; mu_1 = 117.7; G = 1048.3;
mu_sum = mu_knot + mu_1;

%stress level
sigma = 3200;

%extra
mu = (mu_knot*mu_1)/(mu_sum);
Tau = mu/G; %See Chapter 2, this is not Tau1

A = (sigma)/(G);
B = ((mu_1)/(mu_sum))^2;
C = (sigma)/(mu_sum);
D = (mu_1)/(mu_knot);

%time
creep_time = 1; %Total creep time of one second
n_creep = 1000; %Number of points
dt_creep = creep_time/n_creep; %Spacing of points

relax_time = 100; %Allowed up to 1000 seconds of recovery on DSR
n_relax = 10000; %Number of points
dt_relax = relax_time/n_relax; %Spacing of points
---------------------------------------------------


%% Main Code
t(1) = 0; %Intial value

for i = 1:n_creep
    E(i) = (A*B*(1 - exp(-(t(i)/Tau))))+(C*(t(i)));
    Edot(i) = C*(1+(D*exp(-(t(i)/Tau))));
    t(i+1) = t(i) + dt_creep;
end
```

```matlab
%Need +1 to ensure point is calculated for t = 1 second
Emax = (A*B*(1 - exp(-(t(n_creep+1)/Tau))))+(C*(t(n_creep+1)));
Edotmax = C*(1+(D*exp(-(t(n_creep+1)/Tau))));


Ee = (sigma - (mu_knot*Edotmax))/G;
Er = (sqrt(B))*Ee;



for i = (n_creep+1):n_relax
    E(i) = Emax-(Er*(1-exp(-((t(i)-t(n_creep+1))/Tau))));
    t(i+1) = t(i) + dt_relax;
end
%extra because of +1
E(n_relax + 1) = Emax-(Er*(1-exp(-((t(n_relax+1)-1)/Tau))));


%Scaling
Escaled = 100*(E/Emax); %Maximum strain, at 1second, now equals
100%
Predicted_Recovery = 100-(Escaled(length(Escaled)));
--------------------------------------------------


%% Plots

figure('name', 'MSCR Pulse Results')
plot(t,Escaled)
xlim([0 10])%Can choose how much time you want to plot
xlabel('Time, t (seconds)'); ylabel(' Scaled Strain %')
title('PG 70-31P')

%Can import experimental results to get all data
%onto a single figure window.
```